Aerosol water parameterization:
long-term evaluation and importance for climate studies

Swen Metzger[1,2,a], Mohamed Abdelkader[1,2,b], Benedikt Steil[2], and Klaus Klingmüller[2]

[1]Energy, Environment and Water Research Center, The Cyprus Institute, Nicosia, Cyprus
[2]Air Chemistry Department, Max Planck Institute for Chemistry, Mainz, Germany
[a]Now at: ResearchConcepts io GmbH, Freiburg im Breisgau, Germany
[b]Now at: King Abdullah University of Science and Technology, Saudi Arabia

Correspondence: Swen Metzger (swen.metzger@researchconcepts.io)

Abstract.

We scrutinize the importance of aerosol water for the aerosol optical depth (AOD) calculations by a long-term evaluation of the EQuilibrium Simplified Aerosol Model V4 for climate modeling. EQSAM4clim is based on a single solute coefficient approach that efficiently parameterizes hygroscopic growth, accounting for aerosol water uptake from the deliquescence relative humidity up to supersaturation. EQSAM4clim extends the single solute coefficient approach to treat water uptake of multi-component mixtures. The gas-aerosol partitioning and the mixed solution water uptake can be solved analytically, preventing the need for iterations, which is computationally efficient. EQSAM4clim has been implemented in the global chemistry climate model EMAC and compared to ISORROPIA II on climate time-scales. Our global modeling results show that (I) our EMAC results of the aerosol optical depth (AOD) are comparable to modeling results that have been independently evaluated for the period 2000-2010, (II) the results of various aerosol properties of EQSAM4clim and ISORROPIA II are similar and in agreement with AERONET and EMEP observations for the period 2000-2013, and (III) that the underlying assumptions on the aerosol water uptake limitations are important for derived AOD calculations. Sensitivity studies of different levels of chemical aging and associated water uptake show larger effects on AOD calculations for the year 2005 compared to the differences associated with the application of the two gas-liquid-solid partitioning schemes. Overall, our study demonstrates the importance of the aerosol water for climate studies.

1 Introduction

Providing realistic projections of climate change is difficult due to many unknowns and large uncertainties that still exist (Intergovernmental Panel on Climate Change, 2014). For instance, the recent study by Klingmueller et al. (2016) suggests that the observed increase in aerosol optical depth (AOD) over large parts of the Middle East during the period 2001 to 2012 could

5 to some extent prevail as a result of climate change. Even in absence of growing anthropogenic aerosol and aerosol precursor emissions, increasing temperature and decreasing relative humidity, as seen in the last decade, promote soil drying, which can lead to increased dust emissions and hence AOD. Moreover, the discrepancies in the geographical patterns of AOD and aerosol mass measurements can be conclusively explained by aerosol water mass calculations (Nguyen et al., 2016). In fact, also in arid regions the water uptake on dust aerosols becomes important, if air pollution interacts with dust outbreaks (Abdelkader

10 et al., 2015). The uptake of acids on mineral dust can alter the ability of bulk dust to take up water vapor even at a very low ambient relative humidity (RH) – in case of condensing hydrochloric acid (HCl), calcium chloride ($CaCl_2$) can be formed over time which can cause water uptake at a RH as low as 28%. While this might be the case for arid regions all over the Earth, it is not an easy task for climate modelers to correctly quantify the effect due to the complexity of the underlying processes, as indicated by the studies of Abdelkader et al. (2017). To reduce uncertainties, our latter two studies applied the dust emissions

15 scheme of Astitha et al. (2012) together with our chemical speciation of the emissions fluxes (see Section 2.4) in order to resolve a chemical aging of mineral dust particles (see Section 4.2). Furthermore, an interaction of the emission flux with meteorology (Klingmueller et al., 2018) and anthropogenic pollutants, together with a water mass conserving coupling of the aerosol hygroscopic growth into haze and clouds (Metzger and Lelieveld, 2007), is needed.

Proper hygroscopic growth calculations require thermodynamic models that can calculate at least the equilibrium partitioning

20 of aerosols and their precursor gases from different natural sources in interaction with anthropogenic air pollution. To calculate the gas-liquid-solid phase partitioning, a variety of thermodynamic equilibrium models have been therefore developed (Metzger et al. (2016b) and references therein). For instance, MARS (Saxena et al., 1986) is widely used in regional modeling as the thermodynamic core of MADE/SORGAM (Ackermann et al. (1998), Schell et al. (2001)) through applications of the Weather Research and Forecasting model coupled to Chemistry (WRF-Chem, https://ruc.noaa.gov/wrf/wrf-chem/, Ahmadov and Kazil

25 (2018)), the model of the European Monitoring and Evaluation Programme (EMEP, http://www.emep.int/, Simpson et al. (2012)), and the European Air Pollution Dispersion model system (EURAD, http://www.eurad.uni-koeln.de/). On the other side, for climate modeling mainly ISORROPIA (Nenes et al. (1998); Fountoukis and Nenes (2007)) and EQSAM (Metzger et al. (2002b), Metzger et al. (2006)) are widely used because of their computational efficiency. Both codes (among others) were recently used for the investigation of global particulate nitrate as part of the Aerosol Comparisons between Observations

30 and Models (AeroCom) phase III experiment (Bian et al., 2017). Besides this AeroCom study, different EQSAM versions have been used for various other modeling studies, e.g., EQSAM1 (up to EQSAM_v03d): Metzger et al. (2002b), Metzger et al. (2002a), Dentener et al. (2002), Lauer et al. (2005), Tsigaridis et al. (2006), Myhre et al. (2006), Luo et al. (2007), Bauer et al. (2007a) and Bauer et al. (2007b); EQSAM2: Trebs et al. (2005) and Metzger et al. (2006); EQSAM3: Metzger and Lelieveld

(2007) and Bruehl et al. (2012). An overview of widely used modeling systems that provide an option to use either EQSAM and/or ISORROPIA is given in Table 1.

To reduce computational costs, both EQSAM and ISORROPIA follow the MARS approach (Saxena et al. (1986), Binkowski and Shankar (1995)) to determine certain domains by the degree of sulfuric acid neutralization and then divide the relative humidity (RH) and composition space into subdomains to minimize the number of equations to be solved. But in contrast to EQSAM, all other thermodynamic equilibrium models require an iterative procedure to solve the ionic composition, which adds significantly to computational costs.

To accurately parameterise the aerosol hygroscopic growth by also considering the Kelvin effect as described by Metzger et al. (2012), the EQSAM approach (Metzger et al., 2002b)) was recently extended by Metzger et al. (2016b). The new model version, the EQuilibrium Simplified Aerosol Model V4 for climate modeling, enables aerosol water uptake calculations of concentrated nanometer-sized particles up to dilute solutions, i.e. from the compounds relative humidity of deliquescence (RHD) up to supersaturation (Köhler theory). EQSAM4clim extends the single solute coefficient approach of Metzger et al. (2012) to multi-component mixtures, including semi-volatile ammonium compounds and major crustal elements. The advantage of EQSAM4clim is that the entire gas-liquid-solid aerosol phase partitioning and water uptake including major mineral cations (Sec. 2.3), can now be solved analytically without iterations, which potentially can significantly speed-up computations on climate time-scales (Appendix B). Since the thermodynamics of the few widely used equilibrium models such as MARS are limited either to the ammonium-sulfate-nitrate-water system, or only include sodium and chloride but no crustal compounds such as calcium, magnesium and potassium, EQSAM4clim has been evaluated with its introduction against ISORROPIA II at various levels of complexity. It was shown by Metzger et al. (2016b) that the results of EQSAM4clim and ISORROPIA II are similar for reference box-model calculations, textbook examples and 3D applications on time-scales of individual years.

To scrutinize the importance of aerosol water for climate applications, we evaluate the AOD calculations of EQSAM4clim and ISORROPIA II on climate time-scales. For this purpose we extend the model evaluation of (Metzger et al., 2016b) by using the comprehensive chemistry-climate and Earth System model EMAC in a similar setup as applied in our studies on (I) the dust–air pollution dynamics over the eastern Mediterranean (Abdelkader et al., 2015), (II) the sensitivity of transatlantic dust transport to chemical aging and related atmospheric processes (Abdelkader et al., 2017), and (III) the comparison of the Metop PMAp2 AOD products using model data (EUMETSAT ITT 15/210839, Final Report, Metzger et al. (2016a)). These studies employ a highly complex chemistry setup, particularly with respect to the gas-and aqueous phase chemistry and the associated chemical aging of primary aerosols. Since all three studies revealed the importance of chemical aging of primary dust particles for the calculation of the AOD, due to the regional amplification by the aerosol water uptake, it is important to evaluate the aerosol water parameterizion also on climate time-scales. Our EMAC model setup is described in Section 2 and evaluated in Sec. 3 for three periods, 2005, 2000-2010 and 2000-2013 and different model setups that are scrutinized in Sec. 4. Additional results are presented in the Supplement.

2 Model description

2.1 Atmospheric Chemistry-Climate Model EMAC

We use the atmospheric chemistry-climate model EMAC following Abdelkader et al. (2015). EMAC comprises a numerical chemistry and climate simulation system that includes sub-models describing tropospheric and middle atmosphere processes and their interaction with oceans, land and human influences (Joeckel et al. (2005), Joeckel et al. (2006a), Joeckel et al. (2006b), Joeckel et al. (2008), Joeckel et al. (2010), Joeckel et al. (2016)). The core atmospheric model, i.e., the 5th generation European Centre Hamburg general circulation model (ECHAM5, Röckner et al., 2006), is applied with a spherical truncation of T42 and T106 (Gaussian grid of ≈ 2.8 x 2.8^o and ≈ 1.1 x 1.1^o in latitude and longitude) and 31 vertical hybrid pressure levels up to 10 hPa. Our model setup comprises several sub-models that are described below (for details see http://www.messy-interface.org/).

Dry deposition (DDEP) and sedimentation (SEDI) are described by Kerkweg et al. (2006a) and are based on the big leaf approach. Deposition fluxes are calculated as the product of the surface layer concentration and the dry deposition velocity, which reflects the efficiency of the transport to- and destruction at the surface (Ganzeveld et al., 2006). Wet deposition (SCAV) is described by Tost et al. (2006a), while its impact on atmospheric composition is detailed by Tost et al. (2006b) and Tost et al. (2007). The offline (OFFEMIS) and online (ONEMIS) emission calculations, including tracer nudging (TNUDGE), are described by Kerkweg et al. (2006b)), while the sea-air exchange submodel (AIRSEA) calculates the transfer velocity for certain soluble tracers (e.g., methanol, acetone, propane, propene, CO_2 and dimethylsulfide DMS) (Pozzer et al., 2006). The atmospheric chemistry is calculated with the chemistry submodel (MECCA), which was introduced with Sander et al. (2005).

Our chemical mechanism for the troposphere is similar to the one used in Pozzer et al. (2012) – initially described in Joeckel et al. (2006a) (see electronic supplement), although we use a reduced chemistry setup, which consists only of 40 (instead 104) gas phase species and of only 80 (instead 245) chemical reactions. O_3 related chemistry of the troposphere is well included, but we exclude decomposition of non-methane-hydrocarbons (NMHCs) (von Kuhlmann et al., 2003). The other sub-models used in this study are CONVECT (Tost et al., 2006b), LNOX (Tost et al., 2007), as well as CLOUD, CLOUDOPT, CVTRANS, GWAVE, H2O, JVAL, ORBIT, RAD, SURFACE, and TROPOP Joeckel et al. (2010). The aerosol radiative properties (AEROPT) (Pozzer et al. (2012), Klingmueller et al. (2014)) are based on the scheme by Lauer et al. (2007). AEROPT takes the width and mean radii of the lognormal modes into account and considers the composition to obtain the extinction coefficients ($\sigma_{sw,lw}$), single scattering albedo ($\omega_{sw,lw}$) and asymmetry factors ($\gamma_{sw,lw}$) for the shortwave (sw) and longwave (lw) radiation. The radiative forcing is fully coupled in our EMAC version with the primary and secondary aerosols obtained with the GMXe aerosol submodel (Sec. 2.2), which includes the associated water mass thermodynamics (Sec. 2.3), whereby the emission fluxes of primary particles is calculated online in feedback with the EMAC model meteorology (Sec. 2.4).

To represent the actual day-to-day meteorology in the tropospherehe, the model dynamics are weakly nudged (Jeuken et al. (1996), Joeckel et al. (2006a), Lelieveld et al. (2007)) towards the analysis data of the European Centre for Medium-Range Weather Forecasts (ECMWF) operational model data (up to 100 hPa). This allows a direct comparison of our model chemistry with ground station and satellite observations (Sec. 3), by using the anthropogenic emission inventory EDGAR-Climate Change

and Impact Research (CIRCE) Doering et al. (2009a), Doering et al. (2009b), Doering et al. (2009c) on a high spatial (0.1 by 0.1^o) and moderate temporal (monthly) resolution – see e.g., Pozzer et al. (2012) and Pozzer et al. (2017) for details.

2.2 Aerosol Microphysics

Aerosol microphysics and the underlying gas-liquid-solid aerosol partitioning is calculated with the Global Modal-aerosol eX-
5 tension (GMXe) module, which was described by Pringle et al. (2010a) and Pringle et al. (2010b) but originally developed as part of Metzger and Lelieveld (2007). With GMXe we resolve the aerosol size distribution in seven, i.e., four soluble (nucleation, aitken, accumulation and coarse) and three insoluble (aitken, accumulation and coarse) log-normal modes. Primary particles are emitted in the insoluble modes (aitken, accumulation, coarse) and only transferred upon a chemical aging and transport to the respective soluble modes (aitken, accumulation, coarse). Our description of "aging" depends on the amount
10 of available condensable compounds that are the outcome of various emission processes (OFFEMIS, ONEMIS) and chemistry calculations (GMXe, MECCA, SCAV). For the chemical aging of bulk species we follow our approach introduced with Abdelkader et al. (2015), which is scrutinzed in Section 4.2. The condensation dynamics are calculated within GMXe such that coagulation and hygroscopic growth can alter the aerosol the size-distributions. Small particles are efficiently transferred to larger sizes, whereby hygroscopic growth of individual aerosol compounds is calculated from aerosol thermodynamics
15 (Sec. 2.3) based on a chemical speciation of the aerosol emission fluxes (Sec. 2.4). Water uptake of bulk particles (OC, BC, SS, DU), which can be optionally considered, is only treated for aged particles in the soluble modes (Sec. 2.5). Additionally, our EMAC version allows to consider the aerosol hysteresis effect (Sec. 2.6). To avoid an overlap with cloud formation (especially optical thin clouds) the availability of water vapor is dynamically determined within GMXe. This limits the aerosol hygroscopic growth calculation by either ISORROPIA II or EQSAM4clim, described in Sec. 2.3. Through this specific dynamical
20 coupling, our overall water uptake process depends on meteorology and strongly alters with altitude, independently of the aerosol composition.

2.3 Aerosol Thermodynamics

Aerosol thermodynamics is represented by EQSAM4clim (Metzger et al., 2016b) and ISORROPIA II (Fountoukis and Nenes, 2007). Both gas-aerosol partitioning routines calculate the gas-liquid-solid partitioning and aerosol hygroscopic growth. They
25 are embedded in GMXe in exactly the same way, so that a direct comparison of the EMAC modeling results can be made. Deviations can be fully explained by differences in the EQSAM4clim and ISORROPIA II composition calculation approach. Both, EQSAM4clim and ISORROPIA II offer a computationally efficient treatment of the multi-component and multi-phase gas-liquid-solid aerosol partitioning at regional and global scales, by dividing the relative humidity (RH) and composition space into subdomains that minimize the number of equations to be solved. However, the EQSAM4clim framework is based
30 on a single solute specific coefficient (v_i), which was introduced by Metzger et al. (2012) to efficiently parameterise the water uptake of concentrated nanometer-sized particles up to dilute solutions. In contrast to ISORROPIA II, EQSAM4clim covers the mixed solution hygroscopic growth considering the Kelvin effect, i.e. water uptake from the compound's relative humidity of deliquescence (RHD) up to supersaturation (Köhler theory). It was shown by Metzger et al. (2016b) that the ν_i-approach

allows to analytically solve the gas-liquid-solid partitioning and the mixed solution water uptake by eliminating the need for numerical iterations, which can significantly speed-up our EMAC computations (Appendix B). For a consistent model inter-comparison, we limit in this study the gas-aerosol partitioning and associated hygroscopic growth of our EMAC simulations to the inorganic compounds considered by ISORROPIA II. Inorganic aerosol components and their thermodynamic properties

5 used in this study are defined in Table 1 of Metzger et al. (2016b) (with their set-up limited already to match the compounds of ISORROPIA II). Thus, we consider the gas-liquid-solid aerosol partitioning and water uptake of the precursor gases water vapor (H_2O), sulfuric acid (H_2SO_4), nitric acid (HNO_3), hydrochloric acid (HCl), ammonia (NH_3), together with the major cations sodium (Na^+), potassium (K^+), calcium (Ca^{2+}), magnesium (Mg^{2+}), ammonium (NH_4^+), and the major anions sulfate (SO_4^{2-}), bisulfate (HSO_4^-), nitrate (NO_3^-), chloride (Cl^-), such that e.g., nitrate can replace chloride in sea salt aerosols

10 (inline with our EQSAM concept described in Metzger et al. (2002b), Metzger et al. (2002a), Metzger et al. (2006), Metzger and Lelieveld (2007), Metzger et al. (2012), Metzger et al. (2016b), Metzger et al. (2016a)). To enable the full complexity of the phase partitioning with EQSAM4clim and ISORROPIA II, we extend the default EMAC setup through ions assigned to the emission fluxes of primary aerosol particles.

To calculate the aerosol water uptake of bulk species (see Sec. 2.5), we use Eq. A3 of Metzger et al. (2016b). Note that

15 Eq. A3 is an inversion of Eq. (5a) of Metzger et al. (2012), which can be reproduced with the parameters given in Table 2 (with Ke = 1, A = 1, B = 0). As detailed in Sec 2.7 of Metzger et al. (2016b) (p7223), the mixed solution aerosol water uptake can be obtained by their Eq. (22), from tabulated single solute molalities, or parameterised based on Eq. (5a) of Metzger et al. (2012) (Appendix A2, Eq. A3) in agreement with other approaches, including Kappa hygroscopicity parameters (see e.g. Figs. 3 and 4 of Metzger et al. (2016b)). The effect of the implicit assumption (Ke = 1, A = 1, B = 0) on the overall bulk water uptake is

20 negligible for our sensitivity simulations presented in Sec. 4 (studied but not shown).

2.4 Chemical speciation of aerosol emission fluxes

We extend our EMAC setup to include a basic chemical speciation of the natural aerosol emission fluxes in terms of certain cations and/or anions. Usually, climate models treat only bulk tracers such as sea salt (SS), dust (DU), organic carbon (OC) / black carbon (BC). Instead, we assign ions to the bulk emission fluxes of primary aerosols by using the major cations Na^+,

25 K^+, Ca^{2+}, Mg^{2+} and anions SO_4^{2-}, Cl^-. Our concept of chemical speciation was originally developed as part of GMXe by Metzger and Lelieveld (2007) to extend the aerosol water uptake calculations to the so far chemically unresolved bulk aerosol mass. Thus, for bio-mass burning OC and BC aerosols, we consider the potassium cation (K^+) as a key reagent (proxy) for the water uptake thermodynamics (Sec. 2.3). For DU, we respectively consider as a chemical aging proxy the calcium cation (Ca^{2+}), while we resolve the sea salt emission fluxes in terms of the sea water composition, considering the major cations Na^+,

30 K^+, Ca^{2+}, Mg^{2+} and anions Cl^- and SO_4^{2-}. Our emission fluxes of primary sea salt and dust particles are calculated online, in feedback with the EMAC meteorology and radiation computations. Sea salt is emitted in two soluble modes (accumulation and coarse) based on the flux parameterization of Monahan et al. (1986), while mineral dust particles are emitted in two insoluble modes (accumulation and coarse), following Astitha et al. (2012). The required parameters for OC/BC, SS and DU used in our sensitivity study (Sec. 4) to scrutinze the bulk water uptake are given in Table 2 and described in Sec. 2.5. Note that Table 2

gives the fraction of e.g., dust (DU) that is treated as Ca(Cl)$_2$ for the 50% (or as Ca(NO$_3$)$_2$ for the 90%) "aging" case, though being relevant only for bulk water uptake calculations. Respectively, the same is true for sea salt, OC/BC. But this, e.g., DU fraction is not chemically resolved and transported as e.g., Ca(Cl)$_2$, so the overall aerosol composition remains unchanged. This is in contrast to our normal (default) GMXe aging, which is considered in all simulations (Sec. 2.2). Within GMXe, the composition of bulk dust and sea salt is tracked, but the fraction of chemical speciation for the bulk water uptake is prescribed (Table 2). The actual composition is calculated online (Sec. 2.5).

The chemical speciation approach applied in this study was introduced with (Abdelkader et al., 2015) and first applied in Abdelkader et al. (2017). As noted in the former publication (p9176, line 13-16), our chemical speciation has been determined such that the model concentrations best match the available EMEP and CASTNET measurement data for the period 2000-2013 (to be published separately). Publication of the comprehensive model evaluation is foreseen and in progress.

2.5 Chemical aging and water uptake of bulk aerosols

Our chemical speciation of the primary aerosol emission fluxes is coupled to a chemical aging of bulk species through which salt compounds and associated water can be formed. In our model, the uptake of inorganic acids on bulk compounds, and the associated neutralization reactions and water uptake occurs during aerosol transport and thus changes the (bulk) particle hygroscopicity with time. The chemical aging process is hereby based on explizit neutralization reactions of ions (cations, or anions), which are assigned to the emission fluxes (e.g., K$^+$, Ca^{2+}, see Sec. 2.4). Through the reactions of these cations (anions) with aerosol precursor gases, i.e., major oxidation products of natural and anthropogenic air pollution (here H$_2$SO$_4$, HNO$_3$, HCl, NH$_3$, and H$_2$O), various neutralization (salt) compounds can be formed, e.g., potassium sulfate (K$_2$SO$_4$), potassium bisulfate (KHSO$_4$), potassium nitrate (KNO$_3$), potassium chloride (KCl), calcium sulfate (CaSO$_4$), calcium nitrate (Ca(NO$_3$)$_2$), calcium chloride (CaCl$_2$) and so on for ammonium, sodium and magnesium, see Table 1 of Metzger et al. (2016b). The salts can cause an uptake of water vapor (H$_2$O) at different ambient humidities, with CaCl$_2$ at RHs as low as 28%. All salt solutions are subject to the RH and T–dependent gas-liquid-solid partitioning as described in Sec. 2.3 and 2.6. For H$_2$O and each cation and anion, a chemical tracer is assigned such that they undergo all aerosol microphysics and thermodynamic processes for their respective GMXe aerosol mode(s) (Sec. 2.2). Through this tracer coupling, each salt compound can alter the subsequent AOD calculations in our EMAC version, most noticeably through an associated aerosol water uptake.

For the chemical aging our bulk aerosol species (OC/BC, SS and DU), we assume that e.g., bulk OC behaves in terms of water uptake such that it would be coated by ammonium sulfate with an amount of a mass fraction of 50% OC, with the water uptake parameters given in the first sub-column of Table 2. Respectively for the 90% case, ammonium bisulfate is assumed with the water uptake parameters given in the second sub-column (see further explanation in Table 2). To calculate the bulk water uptake, we use the EQSAM4clim parameterizations (introduced by Metzger et al. (2012)) and solve a bulk solute molality using Eq. A3 of Metzger et al. (2016b). For the sake of simplicity, we neglect the Kelvin-term ($K_e = 1$, $A = 1$, $B = 0$) and further assume that the water uptake of the bulk compounds can be described by a mean value, for which we can use our single coefficient ν_i. We further assume a single chemical reagent to be representative for the bulk water uptake due to chemical aging of the bulk aerosol mass, but we only calculate bulk water uptake if the RH exceeds a certain threshold. This "aging" proxy is

given in Table 2 together with the required parameters for our "aging" setup used in Sec. 4.2. For instance, for the "50% aging" case of bulk sea salt mass (SS), we assume $50[\%]$ of the mass to be subject to water uptake if the RH exceeds a threshold of 50%. And for this case we assume NaCl as the proxy with $\nu_i = 1.358$ (Table 1 of Metzger et al. (2016b)). Accordingly, we assume for dust (DU) that 75% of the mass is subject to water uptake if the RH exceeds the threshold of 28%, due to a pre-dominant coating by $CaCl_2$ (with $\nu_i = 2.025$).

To distinguish between our EMAC setup that considers the water uptake of normally chemically unresolved particles (SS, DU, OC, BC), we use in our study the label "$aging$", refering to a chemical "aging" that is used in Sec. 4.2. In contrast, our EMAC setup that omits the chemical "aging" and associated water uptake of bulk aerosols is labeled "$no\ aging$" (Sec. 4.1).

Independent of this "aging" label, all our EMAC simulations consider a comprehensive treatment of the chemical aging of the non-bulk aerosol emission fluxes such that particles can deliquesce or effloresce with age, which is part of our GMXe aerosol dynamical and thermodynamical treatment Sec. 2.2. The chemical aging includes the dynamically limited condensation of aerosol precursor gases on primary aerosol particles. Our primary aerosol particles are emitted in the insoluble modes and, depending on the coating level (i.e., the amount of gases condensed on the insoluble particles), they are transferred to the soluble modes. But only the chemically identified compounds of the soluble modes (aitken, accumulation and coarse mode) are subject to the water uptake calculations by either EQSAM4clim or ISORROPIA II by our "$no\ aging$" set-up. Since the inorganic aerosol composition usually explains only a fraction of the emission fluxes, and since the coating process may involve complicated and largely unknown chemical reactions which alter (age) the aerosol surfaces, we consider for our sensitivity study in Sec. 4 the water uptake of the bulk aerosol mass (as described above). Normally, the bulk aerosol mass would be otherwise considered as dry only. And it was shown by our recent studies by Abdelkader et al. (2015), Metzger et al. (2016b), Metzger et al. (2016a) and Abdelkader et al. (2017) that the results of our EMAC "$aging$" set-up agree better with various ground station observations and satellite measurements.

2.6 Aerosol water mass – hysteresis effect

Our EMAC version further allows to consider the so-called hysteresis effect. That is, we can obtain the aerosol water mass for two cases, i.e, (1) dry case, when RH increases and exceeds the compound's RHD, or mixed solution RHD (Sec. 2.6 of Metzger et al. (2016b)), and (2) wet case, when the RH decreases until crystallization (efflorescence) point of the dissolved compound(s) is reached. Below these thresholds no aerosol water is calculated. The hysteresis effect can become regionally important, since many inorganic salt compounds, which take up water at a given RHD-threshold, do not crystallize at the same threshold. The efflorescence thresholds are often observed to be much lower. Although the hysteresis effect might be less pronounced in ambient observations (simply because the aerosol composition usually changes over time due to transport and chemical reactions), the instantaneous effect on radiation can locally become important.

To consider the hysteresis effect in a climate model, we assume for the sake of simplicity (and because of missing measurements) no single compound efflorescence thresholds. Our criteria that determines a "wet case" or "dry case" instead depends on two factors: (i) an RH threshold and (ii) the existence of aerosol water mass from the previous time-step. In case aerosol water mass from the previous time-step is non-zero for the given time-step (and model grid box), and, if additionally the RH

is above 40% (fixed efflorescence value), we consider the upper hysteresis loop and only calculate the gas-liquid partitioning with either EQSAM4clim or ISORROPIA II. Otherwise, we account for the full gas-liquid-solid partitioning (lower hysteresis loop). The water uptake is then based on deliquescence of single or mixed solutions as described in Metzger et al. (2016b). Note that the aerosol water mass is treated prognostically in our EMAC version Sec. 2.5. That is, we assign a model tracer for water vapor and for each aerosol mode to transport the different water masses. This allows to retrieve the required time information for a certain location on Earth, although we are only approximately able to distinguish between the upper or lower hysteresis loop. Results of our EMAC setup that include the hysteresis effect are shown in Sec. 3 and 4.

3 Climate applications

To evaluate the hygroscopic growth calculations of EQSAM4clim and ISORROPIA II and to evaluate our EMAC version we focus on the AOD, since long-term observations are available for many regions of the Earth. The AOD, or extinction coefficient, is a measure of radiation scattering and absorption at different wavelengths and sensitive to the gas-liquid-solid partitioning and aerosol hygroscopic growth. We use ground-station observations from the AErosol RObotic NETwork (AERONET, http://aeronet.gsfc.nasa.gov). Complementary, we use independent satellite observations from MODIS and MISR (both available from http://disc.sci.gsfc.nasa.gov/giovanni.) The comparison of model results against measurements includes the in-situ observations of the Clean Air Status and Trends NETwork (CASTNET, www.epa.gov/castnet/). CASTNET is a national air quality-monitoring network of the United States of America designed to provide data to assess trends in air quality, atmospheric deposition, and ecological effects due to changes in air pollutant emissions. For Europe, we use data of the European Monitoring and Evaluation Programme (EMEP) (http://www.emep.int/). EMEP is a scientifically based and policy driven program under the Convention on Long-range Transboundary Air Pollution (CLRTAP) for international co-operation to solve transboundary air pollution problems (Tørseth et al., 2012). Our EMAC model evaluation is based on two model resolutions, i.e. T42 and T106 (Sec. 2.1). Most of our model output is based on 5-hourly averages, such that any full hour serves as averaging-interval center once within 5 days. An extension of our study to a more in-depth evaluation of the underlying aerosol composition and neutralization levels will be presented separately, while the sensitivity of the inorganic aerosol composition to model assumptions (e.g. ISORROPIA-II vs EQSAM4clim) is presented in the Supplement of this work (see S1.3, Fig. S6-S20).

3.1 EMAC AOD versus AERONET and Satellites

The EMAC hygroscopic growth calculations of EQSAM4clim and ISORROPIA II are first compared for the period 2000-2010 to independent AOD results of Pozzer et al. (2015) (PO2015). To give a compact but representative picture of our analysis, we focus on a selection of AERONET stations that represent different regions of the Earth. Figure 1 shows the selected station locations, Fig. S1 (Supplement) the corresponding regions. Fig. 2 shows the results of the AOD comparison (from left to right, top to bottom): GSFC (North America), Sao Paulo (South America), Cape San Juan (Latin America), Capo Verde (West Africa), Canberra (Australia), Yekaterinburg (Siberia), Forth Crete (EMME), Dakar (West Africa), Yakutsk (Siberia), Amsterdam Island (Indian Ocean), Lampedusa (North Africa), Beijing (East Asia). Fig. 3 shows the corresponding Taylor diagrams (standard

deviation and correlation coefficient) of the AOD comparison of EQSAM4clim, ISORROPIA II and PO2015. The comparison includes different observations from independent satellite instruments, i.e, MODIS, MODIS-Aqua, MODIS-deep blue, MISR, SeaWIFS and ENVISAT, which are discussed in detail in our extended evaluation study. All satellite products and model results are compared against the AERONET observations for the period 2000-2010 (based on globally averaged seasonal means using

5   a 5 hourly model output and accordingly averaged AERONET observations – details are given in Metzger et al. (2016a), which also outlines our interpolation procedure in time and space). The corresponding scatter plots are shown in Figures S2–S4 of the Supplement and include the statistics: root mean square error (RMSE), correlation coefficient (R), mean biased error (MBE), standard deviation of the model results (σ_m) and AERONET observations (σ_o). The equations are given in Appendix A: Evaluation Metrics.

10   The comparison shows that the differences associated with the two partitioning schemes are smaller compared to the differences associated with the two different EMAC setups, i.e., our EMAC version with EQSAM4clim (orange circles) and ISORROPIA II (blue stars), and the independent PO2015 setup (pink crosses). But all AOD model results are relatively close to the AERONET observations, despite the distinct different underlying approaches to obtain the mixed solution aerosol water uptake. The largest differences occur for regions which are dominated by mineral dust outbreaks, as indicated by the

15   AERONET stations Capo Verde and Dakar (Fig. 2). The reason is that PO2015 uses prescribed dust emissions, while our setup calculates the dust emission fluxes online with the EMAC meteorology (Sec. 2.4). Although the same is true for the sea salt emissions, differences there are much less pronounced (see e.g., Amsterdam Island). The prescribed dust emissions basically yield a mean dust concentration with a too low variability, which is reflected in a too low variability of the AOD results (see pink crosses for e.g. Dakar in Fig. 2). Contrary, our EMAC version results show too low minimum values for certain periods

20   (e.g., for 2002–2008), but the magnitude of the seasonal cycle is much closer to the AERONET observations (black circles). On the other hand, the setup of PO2015 is based on the T106L31 resolution ($\approx$1.1 x 1.1^o), while our results are based on a T42L31 ($\approx$2.8x2.8^o) setup. Although, the coarser resolution somewhat affects the statistics of the analysis (see Supplement), our results are also within the range of the satellite results when compared to the AERONET observations (Figure 3). Notably, spring and summer seasons are for our T42L31 setup better resolved than the winter months. Altogether, the results indicate

25   that we may underestimate the chemical aging of bulk particles, which is therefore scrutinized in Sec. 4.2.

3.2   EQSAM4clim versus ISORROPIA II for 2000–2013

To further evaluate EQSAM4clim and ISORROPIA II, we compare the AOD and the total particulate matter (PM) that drives the model AOD with AERONET and EMEP observations for the period for 2000–2013. Figure 4 shows that the AOD and PM time-series and the climatological year (14 years average) are close to independent observations of the EMEP station Harwell

30   and the AERONET site Chilbolton (United Kingdom, Fig. 1). The two sites lie within one model grid box and are chosen, since no other site provides long-term observations of both AOD and PM. Only Cabauw in the Netherlands, which is one of the few EMEP and AERONET super-sites, provides AOD and PM observations with some reasonable overlap and supports these results as shown in Fig. 5. To complement the picture, the corresponding aerosol water (H_2O), which is associated with

the total model PM, is also shown yielding consistent results for EQSAM4clim and ISORROPIA II (but no observations are available).

Figure S5 in the Supplement (Sec. S1.2) shows the corresponding size-resolved PM, aerosol water, number concentration and wet radius for each aerosol mode: nucleation soluble (ns), aitken soluble (ks), accumulation soluble (as), coarse soluble (cs), aitken insoluble (ki), accumulation insoluble (ai), coarse insoluble (ci); ISORROPIA II (left column), EQSAM4clim (right column). The sum of the modes (for PM, H_2O) is identical to Figure 5 and also supports this finding. Figure 6 further shows various PM time-series of EQSAM4clim and ISORROPIA II (top panels) in comparison with EMEP stations, which provide long-term PM observations, i.e., Cabo de Creus, Hyytiala, Illmitz and Vreedepel. The station locations are shown in Fig. 1, the corresponding climatological year below each time-series (Fig. 6). Interestingly, despite the distinct different regions and climates, our EMAC model results are close to these long-term PM observations. The corresponding global aerosol PM and associated water (H_2O) distributions (14 years average) are shown in Figures 7 and 8: meridional means (left columns), zonal means (middle columns) surface distributions (right columns), ISORROPIA II (ISO2, top rows), EQSAM4clim (EQ4c, middle rows), together with the differences between both simulations (EQ4c–ISO2, bottom rows). Importantly, our water mass results are lowest in the western desert of the U.S. in agreement with e.g., Liao (2005) and Carlton and Turpin (2013).

Important, both the AOD and PM model results nicely compare with various surface observation for the entire evaluation period (2000-2013). But, also the global surface and vertical distributions from both EMAC simulations are in close agreement for the aerosol PM and H_2O, which supports our previous finding (Sec. 3.1) that the difference between EQSAM4clim and ISORROPIA II are negligible on climate simulation time-scales. Figure 9 additionally shows scatter plots of the model AOD versus AERONET observations for the period 2000-2013 and the year 2005. For each period, three different time averages are shown i.e., 5 hourly averages (full time resolution), monthly means and station means based on 537 AERONET stations all over the Earth (locations are shown in Fig. S1 of the Supplement). The statistics included in each panel summarizes the results and show that both EMAC simulations are comparable in terms of statistical key metrics, i.e. Root Mean Square Error (RMSE), Standard deviation (σ), Correlation Coefficient (R), Mean biased Error (MBE) (equations are given in Appendix A). Interestingly, the statistics of all time averages indicate that the results of EQSAM4clim are slightly closer to the AERONET observations compared to ISORROPIA II. Note that Fig. 14 complements Fig. 9 with the results for 2005 by our EMAC "aging" set-up that is discussed further in Sec. 4.2.

3.3 EQSAM4clim versus ISORROPIA II for 2005

In order to scrutinze this result, we zoom into a single location and compare the EMAC AOD of EQSAM4clim and ISORROPIA II for the AERONET observations at Capo Verde for both, 5 hourly and monthly averages (Figure 10). Capo Verde is one of the more difficult stations because of the frequent Sahara dust outflows (Abdelkader et al., 2017). In our setup the dust outflow is associated with elevated calcium loadings, which can cause differences in the subsequent sulfate/bisulfate neutralization (Sec. 4). Despite the slight underestimation of the AOD observations by both model simulations, the results of EQSAM4clim and ISORROPIA II are very close throughout the year. Even the distinct AOD peaks im May, which can be attributed to Saharan dust outbreaks, are well resolved at the 5-hourly output frequency, although the comparison based on

monthly averages seems to be less impressive. Nevertheless, the absolute comparison is overall very good for a chemistry–climate model.

To evaluate the aerosol composition which drives the hygroscopic growth, we further compare our aerosol ammonium (NH_4^+) results against EMEP observations at the measurement site Vredepeel. NH_4^+ is the waekest cation considered in our simulations and driven out of the aerosol phase by all non-volatile cations, because of its semi-volatility. It is one of the most difficult aerosol species to model, if the mineral cations Na^+, K^+, Mg^{2+} and Ca^{2+} are considered, e.g., through a chemical speciation of the aerosol emission fluxes (Sec. 2.4). NH_4^+ therefore shows for cation rich locations the largest sensitivity in our aerosol calculations (shown e.g. by the results of Sec. S1.3 in the Supplement). Only in case NH_4^+ is the only cation that neutralizes the anions SO_4^{2-}, HSO_4^-, NO_3^-, Cl^-, it is preferentially bound with sulfate for which the aerosol concentrations are usually in good agreement with observations. But, including mineral cations through a chemical speciation of emission fluxes, complicates the modeling enormously. Despite these challenges, our comparison with observations in Fig. 11 shows that the total particulate ammonium, i.e., the sum of all liquid and solid NH_4^+ cations, compares well for different time averages for the year 2005. Differences between EQSAM4clim and ISORROPIA II are also rather small for the daily, monthly and even a 14 years monthly mean (climatological year).

To further evaluate our EMAC results on a global scale, Fig. 12 compares the annual mean AOD of ISORROPIA II (left panel) and EQSAM4clim (right panel) against AERONET observations (included as squares) for 2005 (upper and middle row). The upper row represents our "*no aging*" case and excludes chemical aging and hysteresis effects (Sec. 4.1), while the (middle row) represents our "*aging*" case and includes both effects (they are discussed further in Sec. 4.2). The lower row shows independent satellite observations from MODIS and MISR. Altogether, this comparison shows that the EMAC results based on EQSAM4clim and ISORROPIA II are also very similar on a global scale, and that the EMAC results labeled "aging" compare better with the satellite observations than the "no aging" results. This qualitative comparison indicates that the overall assumption on the water uptake is important. But it also shows that the differences between the two different EMAC setups (comparing upper and middle row) are larger than the differences between the two distinct different gas-aerosol partitioning schemes (comparing left and right panels).

4 Sensitivity study (Year 2005)

To scrutinize the importance of the aerosol water calculations we compare our EMAC results in a sensitivity study that excludes (Sec. 4.1) and includes (Sec. 4.2) the aerosol water and bulk water uptake (Sec. 2.5) due to the chemical aging of primary particles (Sec. 2.4).

4.1 EMAC setup – without chemical aging of bulk species

Our EMAC setup without chemical aging omits the water uptake of bulk aerosols (OC, BC, SS, DU) in contrast to the "aging" case (Sec. 4.2), which considers that the bulk particle hygroscopicity can change with time (Sec. 2.5). For both setups we consider the chemical speciation of the emission fluxes (Sec. 2.4) to obtain chemically specified aerosol mass fractions in

terms of cations and anions. But for the "no aging" case, we limit the water uptake to the neutralization products (ion pairs), which are calculated with the partitioning schemes (Sec. 2.3). Our reasoning for this limited setup is that the aerosol water mass of bulk species (Sec. 2.5), as well as the hysteresis effect (Sec. 2.6), can regionally reduce potential differences of the aerosol water mass calculations, if the total aerosol water mass is dominated by one of these effects. For both processes explicit

5 RHD calculations and the associated uncertainties (Metzger et al., 2016b) are excluded. The "no aging" setup is therefore most sensitive to potential differences in the water uptake calculation approaches of EQSAM4clim and ISORROPIA II, though differences are rather small on a global scale as discussed in Sec. 3.3 (i.e., shown by the comparison in Fig. 12, upper panels).

We note that the relatively largest deviations occur in our "no aging" EMAC setup for stations that are subject to high dust loads, e.g., Dakar and Capo Verde (see Supplement). But the aerosol properties that are most important for climate modelling,

10 i.e., the total (dry) PM and the associated aerosol water mass concentrations are mostly close to a one-by-one line for all simulations and all stations. Differences are mainly caused by differences in the bisulfate / sulfate partitioning of both schemes. In contrast to ISORROPIA II, EQSAM4clim does not treat the dissolution of weak acids (HNO_3, HCl) and bases (NH_3), which can cause differences in the sulfate neutralization levels and the subsequent water coating of mineral dust particles. Also the Kelvin effect is not considered in ISORROPIA II in contrast to EQSAM4clim, which can have an effect on the water uptake

15 of Aitken mode but not coarser particles. Nevertheless, overall differences are small in terms of mass concentrations as shown by the extended analysis included in the Supplement.

Note that the Supplement (Sec. S1.3) shows both time series and scatter plots for 2005 for our "no aging" case which are based on all 537 AERONET stations of Fig. 1. The results include the PM (Fig. S6) and H_2O (Fig. S7) concentrations $[\mu g/m^3 (air)]$, as well as those of the lumped aerosols, i.e., sulfate (SO_4^{2-}), bisulfate (HSO_4^-), nitrate (NO_3^-), chloride (Cl^-),

20 ammonium (NH_4^+), sodium (Na^+), potassium (K^+), magnesium (Mg^{2+}) and calcium (Ca^{2+}); shown in Figs. S8–S16. The corresponding scatter plots Fig. S17 – S20 show the annual means for three soluble (key) aerosol modes of GMXe (Sec. 2.2): coarse (top row), accumulation (middle row) and aitken (bottom row) and include the growth factor (GF, see Metzger et al. (2016b)). Each panel includes the statistics: Root Mean Square Error (RMSE), Correlation Coefficient (R), Mean biased Error (MBE), Standard deviation of ISORROPIA II (x-STD) and EQSAM4clim (y-STD). Table 3 complements the time series and

25 scatter plots with some additional statistics of key EMAC tracers.

4.2 EMAC setup – with chemical aging of bulk species

The EMAC setup labeled "aging" extends the "no aging" setup (Sec. 4.1) by the water mass calculation of bulk aerosol species and the hysteresis effect (Sec. 2.6) such that the bulk particle hygroscopicity can change with time (Sec. 2.5) – note Table 4. Both can become regionally important. As noted in Sec. 3.3, our EMAC "aging" setup compares better with observations than

30 the "no aging" case. This is especially true for regions over the open oceans, intense bio-mass burnings or dust outbreaks, including the transatlantic dust transport as shown in Fig. 12. But despite the more complex chemical aging setup of bulk species, our EMAC version still somewhat underestimates the AOD observations. This finding is supported by the AERONET observations, which are included in Fig. 12 (squares with the same color scale). One reason could be that our default "aging" set-up only considers a partial "aging" of 50% of the bulk aerosol mass for the additional water uptake calculations.

To scrutinize the effect of "aging level" on the AOD comparison, we apply different levels of bulk "aging" according to Table 4. Figure 13 shows the results of four different EMAC simulations, i.e., case 1: "no aging" (blue stars), case 2: "no water" (orange circles), case 3: "50% aging" (pink crosses), case 4: "90% aging" (light blue squares). The upper two rows compare the model results of EQSAM4clim and ISORROPIA II based on case 4 for the AERONET observations at Lampedusa and Beijing for the year 2005. The first and third row show the 5 hourly means, while the 2nd and 4th row show the corresponding monthly means. The lowest two rows present the key-results of our sensitivity study.

The comparison of the cases 1–4 shows that aerosol water calculations are essential. Excluding "aging" or aerosol water at all, our EMAC simulation largely underestimates the AOD (case 1–2), while considering the bulk water uptake ("aging" case 3–4) improves the AOD comparison. But, the improvement strongly depends on the AERONET location and the assumed level of "aging". For instance, our EMAC results based on a 90% "aging" level (case 4) can overestimate the AOD observations at certain locations such as for Lampedusa, while at the same time the results compare best with other observations such at the AERONET site of Beijing. With a decreasing level of "aging", the AOD observations get more underestimated for Beijing, while improved for Lampedusa. This fact points to missing processes that cannot be resolved by applying constant chemical aging parameters. To improve our results further, a more comprehensive chemical aging parameterization is needed by e.g., an extension of the water uptake framework to organic compounds as considered by Metzger and Lelieveld (2007). The latter study included the neutralization of major carboxylic acids for the neutralisation by the cations Na^+, K^+, Ca^{2+}, Mg^{2+} to form salt compounds (formates, acetates, oxalates, citrates, see their Table 1), which can contribute to the overall aerosol water mass and hence regionally improve the AOD. Yet, such extensions are beyond the scope of this work. Here, we focus on a consistent model-inter comparison of EQSAM4clim and ISORROPIA II and the importance of aerosol water mass for the model evaluation in terms of AOD. Nevertheless, our EMAC results based on the higher "aging" level (case 4) improve the global scale comparison of Fig. 9 (discussed in Sec. 3.2) as shown by Fig. 14. Note that the hysteresis assumption (Sec. 2.6) comes on top of both, i.e., our "aging" and "no aging" (Sec. 4.1) assumption, but is negligible in our EMAC set-up compared to the "aging" effect, which is why we have not separated it from the sensitivity analysis. So, the differences in AOD between "aging" and "no aging" are basically caused by the associated water uptake of bulk compounds (SS, DU, OC, BC).

Overall, our sensitivity analysis indicates the potential limitations associated with the lack of water uptake on organic aerosol, the effects of organic aerosol on inorganic partitioning and resulting water uptake, and water uptake and resulting AOD. With Fig. 13 we show the results of different "aging" assumptions. Although we do not explicitly treat organic aerosols, the 50 and 90% aging case also includes water uptake of organic aerosols through our consideration of OC bulk mass (with the parameters given in Table 2). Clearly, only certain regions are dominated by organic aerosols and the water uptake of organic aerosols is usually much less than those of the inorganic counterparts (if normalized to the aerosol mass). Nevertheless, certain regions such as Beijing can be dominated by organic aerosols and the effect on AOD can be significant as shown by Fig. 13 – compare "no water" without aerosol water (orange circles), "50% aging" (pink crosses), "90% aging" (light blue squares) for the monthly means, lowest right panel.

4.3 Importance of Aerosol Water

The sensitivity of our AOD calculations with respect to the RH cut-off is analyzed next. Such a cut-off is required for all aerosol water mass calculations and applied to prevent overlap between aerosol hygroscopic growth and parameterized cloud formation. Most of our EMAC simulations use a default cutoff of (maximum) RH=95 or 98%, while there is no minimum RH by default. In our EMAC simulations the minimum RH is determined automatically by the aerosol composition, i.e., by the single solute or mixed solution deliquescence RH (this is detailed in Sec 2.6 of Metzger et al. (2016b)).

Here we consider four different RH cut-off cases for which AOD results (2005, annual mean) of four EMAC simulations are shown in Figure 15 (from left to right, top to bottom): (UL) RH= 0[%], i.e., no aerosol water, (UR) RH= 97[%], (LL) RH= 98[%], and (LR) RH= 99.9[%]. The four simulations only differ by the assumption on the aerosol water uptake limitation, i.e., the upper RH value that is used to limit the water uptake calculation for both EQSAM4clim and ISORROPIA II. While our first and last sensitivity simulations represent an extreme case (with unrealistic AOD results), the two simulations with RH= 97 and 98[%] cut-offs yield similar AOD results that are relatively close to many AERONET observations (colored squares). Noticeably, the AOD values significantly increase for the high RH= 99.9[%] case. Of course, any RH cut-off is arbitrary, if the aerosol water mass is not consistently linked with cloud formation. To avoid an inconsistent aerosol-cloud-radiation coupling, Metzger and Lelieveld (2007) proposed a mass conservative coupling approach to limit the aerosol water mass by an approach that needs to be further scrutinzed too (presented elsewhere).

5 Conclusions

The importance of aerosol water for AOD calculations has been scrutinized by a long-term evaluation of EQSAM4clim and ISORROPIA II on climate time-scales using our EMAC model version as applied in Abdelkader et al. (2015), Metzger et al. (2016b) and Abdelkader et al. (2017). Generally, the results of both gas-liquid-solid partitioning schemes are in good agreement despite differences in the bisulfate partitioning and mixed solution deliquescence humidity range, where the results of thermodynamic schemes are typically associated with deviations (Metzger et al., 2016b). However, these discrepancies are negligible for climate simulations, as the total aerosol water mass and AOD do not significantly differ. Furthermore, besides the relative importance of (a) the general model setup (EQSAM4clim or ISORROPIA II), (b) number and types of compounds considered for the aerosol water calculations (e.g., mineral cations), (c) water uptake by bulk species and chemical aging, (d) hysteresis effect (efflorescence versus deliquescence), it appeared that (e) the aerosol water uptake limitations of both partitioning schemes is most determinant for AOD calculations. Overall, the comparison of our EMAC results with remote sensing AOD observations reveals the importance of the aerosol water calculations for climate applications.

Acknowledgements. This work was supported by the European Research Council under the European Union's Seventh Framework Programme (FP7/2007-2013)–ERC grant agreement no. 226144 through the C8-Project, and by the Energy oriented Centre of Excellence (EoCoE), grant agreement number 676629, funded within the Horizon2020 framework of the European Union. EMAC simulations have

been carried out on the supercomputer of the German Climate Research Center and on the Cy-Tera Cluster, operated by the Cyprus Institute (CyI) and co-funded by the European Regional Development Fund and the Republic of Cyprus through the Research Promotion Foundation (Project Cy-Tera NEA-$Y\Pi O\Delta OMH/\Sigma TPATH$/0308/31). Model emissions were kindly provided by the anthropogenic emission inventory EDGAR-Climate Change and Impact Research (CIRCE) through the EU FP6 project No. 036961. We thank the measurement and model development teams for providing the observations, numerical models and the many useful codes that have been used in this study.

Appendix A: Evaluation metrics

Root Mean Square Error:

$$RMSE = \sqrt{\frac{1}{N} \sum (X_m - X_o)^2} \tag{A1}$$

Standard deviation:

$$\sigma = \sqrt{\frac{1}{N} \sum_{i=1}^{N} (X_i - \bar{X})^2}, \qquad where \quad \bar{X} = \frac{1}{N} \sum_{i=1}^{N} X_i \tag{A2}$$

Correlation coefficient:

$$R = \frac{\sum_{i=1}^{N} (X_i^m - \bar{X^m})(X_i^o - \bar{X^o})}{\sqrt{\sum_{i=1}^{N} (X_i^m - \bar{X^m})^2 \sum_{i=1}^{N} (X_i^o - \bar{X^o})^2}} \tag{A3}$$

Mean biased Error (MBE):

$$MBE = \frac{1}{N} \sum (X_m - X_o) \tag{A4}$$

10   Index m refers to EQSAM4clim (EQ4c) and o to ISORROPIA II (ISO2).

Appendix B: Computational Efficiency

Computational efficiency is a key-constraint on our model development. To scrutinize the model performance, we compare both gas-aerosol partitioning schemes (EQSAM4clim and ISORROPIA II) using the simulation period of 2005. Table 5 presents the computational burden (CPU times) for different EMAC simulations (T42L31). Experiments A, B, C and D correspond to

15   a "$no\ aging$" EMAC setup (results of Exp A and B are shown in Sec. S1.3 of the Supplement). The four simulations only differ by the constraint on the gas/aerosol partitioning scheme, i.e., Exp A represents ISORROPIA II, Exp B and C represent two simulations of EQSAM4clim (identical setup, just quantifying numerical noise of the computing architecture), while for Exp D the call to the gas-liquid-solid partitioning scheme has been commented out, while all other GMXe processes remained unchanged (Sec. 2.2). Exp D therefore represents the minimum of CPU time that is required for our GMXe aerosol setup on the

20   Cy-Tera super computer (https://cytera.cyi.ac.cy/). Two additional experiments, labeled Exp A_0 and B_0, represent sensitivity simulations of ISORROPIA II and EQSAM4clim, respectively. Both only omit anthropogenic emissions in our EMAC set up, while all other EMAC processes remained the same as for Exp A and B.

Table 5 reveals the real CPU-utilization. The comparison of the numbers shows: (i) a dependency of both partitioning schemes on the aerosol setup and composition (Exp A versus A_0 and B versus B_0), (ii) that the dependency of the additional

25   computational costs for EQSAM4clim besides GMXe is small (Exp B and C versus D and B_0 versus D), while (iii) this is not that much the case for ISORROPIA II (Exp A versus D and A_0 versus D). Given the uncertainty in these numbers due to the different system loads (indicated by Exp B versus C), the additional computational cost of EQSAM4clim is clearly negligible

for climate applications on architecture such as of the Cy-Tera cluster (Intel Westmere X5650 processors, 2 hexa-core sockets per node). But the differences depend on the system and its usage and are generally smaller on pure scalar architectures. On typical vector machines, however, these differences can significantly increase, since the optimization of a short code can be much more effective. For instance, for the previous supercomputer system at the German Climate Research Center (DKRZ,

5 www.dkrz.de), the gain in CPU time has been about an order of magnitude. The fraction of the total EMAC CPU burden for a 2 months simulation was for ISORROPIA II about 20 %, while EQSAM4clim contributed less than 2 % (both on 128 CPUs @ "Blizzard", i.e., IBM Power6 and measured with SCALASCA, http://www.scalasca.org/).

EQSAM4clim has the advantage of being a short fortran 90 code with approximately 850 lines, including comments (or about 8 pages, see Appendix of Metzger et al. (2016b)). For comparison, ISORROPIA II roughly counts 36,300 lines (or

10 approx. 360 pages). This is about 1/3 of the entire source code of the EMAC underlying climate code (ECHAM5.3.02), which has about 119,900 lines of f90 code (also including comments). It should be emphasized that ISORROPIA II was developed for air quality rather than climate modeling, and we offer EQSAM4clim as an alternative for computationally demanding climate simulations.

Appendix C: Code availability

15 EQSAM4clim is freely available for research and non-commercial applications. For commercial applications a special licensing applies. For both cases, please contact the author (swen.metzger@researchconcepts.io). The Modular Earth Submodel System (MESSy) is continuously further developed and applied by a consortium of institutions. The usage of MESSy and access to the source code is licensed to all affiliates of institutions which are member of the MESSy Consortium. Institutions can be member of the MESSy consortium by signing the MESSy Memorandum of Understanding. More information can be

20 found on the MESSy Consortium Website (http://www.messy-interface.org/).

References

Abdelkader, M., Metzger, S., Mamouri, R. E., Astitha, M., Barrie, L., Levin, Z., and Lelieveld, J.: Dust-air pollution dynamics over the eastern Mediterranean, Atmos. Chem. Phys., 15, 9173–9189, https://doi.org/10.5194/acp-15-9173-2015, http://www.atmos-chem-phys.net/15/9173/2015/, 2015.

5   Abdelkader, M., Metzger, S., Steil, B., Klingmueller, K., Tost, H., Pozzer, A., Stenchikov, G., Barrie, L., and Lelieveld, J.: Sensitivity of transatlantic dust transport to chemical aging and related atmospheric processes, Atmos. Chem. Phys., 17, 3799–3821, https://doi.org/10.5194/acp-17-3799-2017, https://www.atmos-chem-phys.net/17/3799/2017/, 2017.

Ackermann, I. J., Hass, H., Memmesheimer, M., Ebel, A., Binkowski, F. S., and Shankar, U.: Modal aerosol dynamics model for Europe, Atmos. Environ., 32, 2981–2999, https://doi.org/10.1016/S1352-2310(98)00006-5, http://linkinghub.elsevier.com/retrieve/pii/
10   S1352231098000065, 1998.

Ahmadov, R. and Kazil, J.: Aerosol modeling with WRF-Chem, Tutorial WRF-Chem Tutorial, CU CIRES and NOAA Earth System Research Laboratory, https://ruc.noaa.gov/wrf/wrf-chem/wrf_tutorial_2018/Aerosols.pdf, 2018.

Astitha, M., Lelieveld, J., Abdel Kader, M., Pozzer, A., and de Meij, A.: Parameterization of dust emissions in the global atmospheric chemistry-climate model EMAC: impact of nudging and soil properties, Atmos. Chem. Phys., 12, 11 057–11 083,
15   https://doi.org/10.5194/acp-12-11057-2012, http://www.atmos-chem-phys.net/12/11057/2012/, 2012.

Bauer, S. E., Koch, D., Unger, N., Metzger, S. M., Shindell, D. T., and Streets, D. G.: Nitrate aerosols today and in 2030: a global simulation including aerosols and tropospheric ozone, Atmos. Chem. Phys., 7, 5043–5059, https://doi.org/10.5194/acp-7-5043-2007, http://www.atmos-chem-phys.net/7/5043/2007/, 2007a.

Bauer, S. E., Mishchenko, M. I., Lacis, A. A., Zhang, S., Perlwitz, J., and Metzger, S. M.: Do sulfate and nitrate coatings on mineral
20   dust have important effects on radiative properties and climate modeling?, J. Geophys. Res., 112, https://doi.org/10.1029/2005JD006977, http://www.agu.org/pubs/crossref/2007/2005JD006977.shtml, 2007b.

Bessagnet, B., Hodzic, A., Vautard, R., Beekmann, M., Cheinet, S., Honoré, C., Liousse, C., and Rouil, L.: Aerosol modeling with CHIMERE—preliminary evaluation at the continental scale, Atmos. Environ., 38, 2803–2817, https://doi.org/10.1016/j.atmosenv.2004.02.034, http://linkinghub.elsevier.com/retrieve/pii/S1352231004002110, 2004.

25   Bian, H., Chin, M., Hauglustaine, D. A., Schulz, M., Myhre, G., Bauer, S. E., Lund, M. T., Karydis, V. A., Kucsera, T. L., Pan, X., Pozzer, A., Skeie, R. B., Steenrod, S. D., Sudo, K., Tsigaridis, K., Tsimpidi, A. P., and Tsyro, S. G.: Investigation of global particulate nitrate from the AeroCom phase III experiment, Atmos. Chem. Phys., 17, 12 911–12 940, https://doi.org/10.5194/acp-17-12911-2017, https://www.atmos-chem-phys.net/17/12911/2017/, 2017.

Binkowski, F. S. and Shankar, U.: The Regional Particulate Matter Model: 1. Model description and preliminary results, J. Geophys. Res.,
30   100, 26 191, https://doi.org/10.1029/95JD02093, http://doi.wiley.com/10.1029/95JD02093, 1995.

Bruehl, C., Lelieveld, J., Crutzen, P. J., and Tost, H.: The role of carbonyl sulphide as a source of stratospheric sulphate aerosol and its impact on climate, Atmos. Chem. Phys., 12, 1239–1253, https://doi.org/10.5194/acp-12-1239-2012, http://www.atmos-chem-phys.net/12/1239/2012/, 2012.

Carlton, A. G. and Turpin, B. J.: Particle partitioning potential of organic compounds is highest in the Eastern US and driven by anthropogenic
35   water, Atmos. Chem. Phys., 13, 10 203–10 214, https://doi.org/10.5194/acp-13-10203-2013, https://www.atmos-chem-phys.net/13/10203/2013/, 2013.

Darmenov, A., da Silva, A., Colarco, P., Gelaro, R., Todling, R., Bian, H., Longo, K., Castellanos, P., Nielsen, E., Buchard-Marchant, V., Randles, C., and Keller, C.: NASA Update GEOS-5 Model and Data Assimilation System: Aerosols and Clouds prsented at the International Cooperative for Aerosol Prediction (ICAP/AEROCAST) "Lidar Data and its use in Model Verification and Data Assimilation", July 12-14, 2016, College Park, MD, USA, http://icap.atmos.und.edu/ICAP8/Day1/Darmenov_TuesdayPM.pdf, 2016.

5 de Meij, A., Krol, M., Dentener, F., Vignati, E., Cuvelier, C., and Thunis, P.: The sensitivity of aerosol in Europe to two different emission inventories and temporal distribution of emissions, Atmos. Chem. Phys., 6, 4287–4309, https://doi.org/10.5194/acp-6-4287-2006, http://www.atmos-chem-phys.net/6/4287/2006/, 2006.

de Meij, A., Pozzer, A., Pringle, K., Tost, H., and Lelieveld, J.: EMAC model evaluation and analysis of atmospheric aerosol properties and distribution with a focus on the Mediterranean region, Atmos. Res., 114-115, 38–69, https://doi.org/10.1016/j.atmosres.2012.05.014, 10 http://linkinghub.elsevier.com/retrieve/pii/S0169809512001536, 2012.

de Meij, A.: Uncertainties in modelling the spatial and temporal variations in aerosol concentrations, https://doi.org/10.6100/IR642890, https://bit.ly/2DXTIJh, 2009.

Dentener, F., Williams, J., and Metzger, S.: Aqueous Phase Reaction of HNO4: The Impact on Tropospheric Chemistry, J. Atmos. Chem., 41, 109–134, https://doi.org/10.1023/A:1014233910126, 2002.

15 Doering, U. M., Monni, S., Pagliari, V., Orlandini, L., van Aardenne, J., and SanMartin, F.: CIRCE report D8.1.1: Emission inventory for the past period 1990–2005 on 0.1x0.1 grid, Tech. rep., Project FP6: 6.3 No. 036961, Joint Research Centre (JRC), http://edgar.jrc.ec.europa.eu/overview.php?v=432_GHG&SECURE=123, 2009a.

Doering, U. M., van Aardenne, J., Monni, S., Pagliari, V., Orlandini, L., and SanMartin, F.: CIRCE report D8.1.2 – Evaluation emission database 1990–2005, Tech. rep., Project FP6: 6.3 No. 036961, Joint Research Centre (JRC), http://edgar.jrc.ec.europa.eu/overview.php?20 v=432_GHG&SECURE=123, 2009b.

Doering, U. M., van Aardenne, J., Monni, S., Pagliari, V., Orlandini, L., and SanMartin, F.: CIRCE report D8.1.3 – Update of grid- ded emission inventories, addition of period 1990–1999 to 2000- 2005 dataset, Tech. rep., Project FP6: 6.3 No. 036961, Joint Research Centre (JRC), http://edgar.jrc.ec.europa.eu/overview.php?v=432_GHG&SECURE=123, 2009c.

Environ, R.: User's Guide COMPREHENSIVE AIR QUALITY MODEL WITH EXTENSIONS Version 6.40, Tech. rep., Ramboll, 773 San 25 Marin Dr., Suite 2115, Novato, CA 94945, USA, 773 San Marin Drive, Suite 2115 Novato, California, 94998, www.ramboll.com,www.camx.com, 2016.

Fountoukis, C. and Nenes, A.: ISORROPIA II: a computationally efficient thermodynamic equilibrium model for K+, Ca2+, Mg2+, NH4+, Na+, SO42-, NO3-, Cl-, H2O aerosols, Atmos. Chem. Phys., 7, 4639–4659, https://doi.org/10.5194/acp-7-4639-2007, http://www.atmos-chem-phys.net/7/4639/2007/, 2007.

30 Ganzeveld, L. N., van Aardenne, J. A., Butler, T. M., Lawrence, M. G., Metzger, S. M., Stier, P., Zimmermann, P., and Lelieveld, J.: Technical Note: Anthropogenic and natural offline emissions and the online EMissions and dry DEPosition submodel EMDEP of the Modular Earth Submodel system (MESSy), Atmos. Chem. Phys. Discussions, 6, 5457–5483, https://doi.org/10.5194/acpd-6-5457-2006, http://www.atmos-chem-phys-discuss.net/6/5457/2006/, 2006.

Intergovernmental Panel on Climate Change, ed.: Climate Change 2013 - The Physical Science Basis: Working Group I Contribu- 35 tion to the Fifth Assessment Report of the Intergovernmental Panel on Climate Change, Cambridge University Press, Cambridge, https://doi.org/10.1017/CBO9781107415324, http://ebooks.cambridge.org/ref/id/CBO9781107415324, 2014.

Jeuken, A. B. M., Siegmund, P. C., Heijboer, L. C., Feichter, J., and Bengtsson, L.: On the potential of assimilating meteorological analyses in a global climate model for the purpose of model validation, J. Geophys. Res.: Atmospheres, 101, 16 939–16 950, https://doi.org/10.1029/96JD01218, http://doi.wiley.com/10.1029/96JD01218, 1996.

Joeckel, P., Sander, R., Kerkweg, A., Tost, H., and Lelieveld, J.: Technical Note: The Modular Earth Submodel System (MESSy) - a new approach towards Earth System Modeling, Atmos. Chem. Phys., 5, 433–444, https://doi.org/10.5194/acp-5-433-2005, http://www.atmos-chem-phys.net/5/433/2005/, 2005.

Joeckel, P., Tost, H., Pozzer, A., Bruehl, C., Buchholz, J., Ganzeveld, L., Hoor, P., Kerkweg, A., Lawrence, M., Sander, R., Steil, B., Stiller, G., Tanarhte, M., Taraborrelli, D., van Aardenne, J., and Lelieveld, J.: The atmospheric chemistry general circulation model ECHAM5/MESSy1: consistent simulation of ozone from the surface to the mesosphere, Atmos. Chem. Phys., 6, 5067–5104, https://doi.org/10.5194/acp-6-5067-2006, http://www.atmos-chem-phys.net/6/5067/2006/, 2006a.

Joeckel, P., Tost, H., Pozzer, A., Bruehl, C., Buchholz, J., Ganzeveld, L., Hoor, P., Kerkweg, A., Lawrence, M. G., Metzger, S., Sander, R., Steil, B., Stiller, G., Tanarhte, M., Taraborrelli, D., van Aardenne, J., and Lelieveld, J.: Evaluation of the atmospheric chemistry general circulation model ECHAM5/MESSy1, http://adsabs.harvard.edu/abs/2006AGUFM.A51B0073J, 2006AGUFM.A51B0073J, Provided by the SAO/NASA Astrophysics Data System, 2006b.

Joeckel, P., Kerkweg, A., Buchholz-Dietsch, J., Tost, H., Sander, R., and Pozzer, A.: Technical Note: Coupling of chemical processes with the Modular Earth Submodel System (MESSy) submodel TRACER, Atmos. Chem. Phys., 8, 1677–1687, https://doi.org/10.5194/acp-8-1677-2008, http://www.atmos-chem-phys.net/8/1677/2008/, 2008.

Joeckel, P., Kerkweg, A., Pozzer, A., Sander, R., Tost, H., Riede, H., Baumgaertner, A., Gromov, S., and Kern, B.: Development cycle 2 of the Modular Earth Submodel System (MESSy2), Geosci. Model Dev., 3, 717–752, https://doi.org/10.5194/gmd-3-717-2010, http://www.geosci-model-dev.net/3/717/2010/gmd-3-717-2010.html, 2010.

Joeckel, P., Tost, H., Pozzer, A., Kunze, M., Kirner, O., Brenninkmeijer, C. A. M., Brinkop, S., Cai, D. S., Dyroff, C., Eckstein, J., Frank, F., Garny, H., Gottschaldt, K.-D., Graf, P., Grewe, V., Kerkweg, A., Kern, B., Matthes, S., Mertens, M., Meul, S., Neumaier, M., Nuetzel, M., Oberländer-Hayn, S., Ruhnke, R., Runde, T., Sander, R., Scharffe, D., and Zahn, A.: Earth System Chemistry integrated Modelling (ESCiMo) with the Modular Earth Submodel System (MESSy) version 2.51, Geosci. Model Dev., 9, 1153–1200, https://doi.org/10.5194/gmd-9-1153-2016, http://www.geosci-model-dev.net/9/1153/2016/, 2016.

Kaiser, J. C., Hendricks, J., Righi, M., Riemer, N., Zaveri, R. A., Metzger, S., and Aquila, V.: The MESSy aerosol submodel MADE3 (v2.0b): description and a box model test, Geosci. Model Dev., 7, 1137–1157, https://doi.org/10.5194/gmd-7-1137-2014, http://www.geosci-model-dev.net/7/1137/2014/, 2014.

Karydis, V. A., Tsimpidi, A. P., Pozzer, A., Astitha, M., and Lelieveld, J.: Effects of mineral dust on global atmospheric nitrate concentrations, Atmos. Chem. Phys., 16, 1491–1509, https://doi.org/10.5194/acp-16-1491-2016, https://www.atmos-chem-phys.net/16/1491/2016/, 2016.

Kerkweg, A., Buchholz, J., Ganzeveld, L., Pozzer, A., Tost, H., and Joeckel, P.: Technical Note: An implementation of the dry removal processes DRY DEPosition and SEDImentation in the Modular Earth Submodel System (MESSy), Atmos. Chem. Phys., 6, 4617–4632, https://doi.org/10.5194/acp-6-4617-2006, http://www.atmos-chem-phys.net/6/4617/2006/, 2006a.

Kerkweg, A., Sander, R., Tost, H., and Joeckel, P.: Technical note: Implementation of prescribed (OFFLEM), calculated (ONLEM), and pseudo-emissions (TNUDGE) of chemical species in the Modular Earth Submodel System (MESSy), Atmos. Chem. Phys., 6, 3603–3609, https://doi.org/10.5194/acp-6-3603-2006, http://www.atmos-chem-phys.net/6/3603/2006/, 2006b.

Klingmueller, K., Steil, B., Bruehl, C., Tost, H., and Lelieveld, J.: Sensitivity of aerosol radiative effects to different mixing assumptions in the AEROPT 1.0 submodel of the EMAC atmospheric-chemistry–climate model, Geosci. Model Dev., 7, 2503–2516, https://doi.org/10.5194/gmd-7-2503-2014, http://www.geosci-model-dev.net/7/2503/2014/, 2014.

Klingmueller, K., Pozzer, A., Metzger, S., Stenchikov, G. L., and Lelieveld, J.: Aerosol optical depth trend over the Middle East, Atmos. Chem. Phys., 16, 5063–5073, https://doi.org/10.5194/acp-16-5063-2016, http://www.atmos-chem-phys.net/16/5063/2016/, 2016.

Klingmueller, K., Metzger, S., Abdelkader, M., Karydis, V. A., Stenchikov, G. L., Pozzer, A., and Lelieveld, J.: Revised mineral dust emissions in the atmospheric chemistry-climate model EMAC (MESSy 2.52 DU_Astitha1 KKDU2017 patch), Geosci. Model Dev., 11, 989–1008, https://doi.org/10.5194/gmd-11-989-2018, https://www.geosci-model-dev.net/11/989/2018/, 2018.

Koo, B., Wilson, G. M., Morris, R. E., Dunker, A. M., and Yarwood, G.: Comparison of Source Apportionment and Sensitivity Analysis in a Particulate Matter Air Quality Model, Environ. Sci. Technol., 43, 6669–6675, https://doi.org/10.1021/es9008129, http://pubs.acs.org/doi/abs/10.1021/es9008129, 2009.

Koo, B., Metzger, S., Emery, C., Wilson, G., and Yarwood, G.: Comparing the ISORROPIA and EQSAM Aerosol Thermodynamic Options in CAMx - ITM 2018 - 36 TH INTERNATIONAL TECHNICAL MEETING ON AIR POLLUTION MODELLING AND ITS APPLICATION, 14 - 18 MAY 2018, THE LORD ELGIN HOTEL, OTTAWA, CANADA, (IN CONJUNCTION WITH THE ANNUAL WMO-GURME MEETING), https://itm2018.vito.be, [1] Ramboll, 773 San Marin Dr., Suite 2115, Novato, CA 94945, USA, [2] ResearchConcepts io GmbH, Freiburg im Breisgau, Germany, 2018.

Lac, C., Chaboureau, J.-P., Masson, V., Pinty, J.-P., Tulet, P., Escobar, J., Leriche, M., Barthe, C., Aouizerats, B., Augros, C., Aumond, P., Auguste, F., Bechtold, P., Berthet, S., Bieilli, S., Bosseur, F., Caumont, O., Cohard, J.-M., Colin, J., Couvreux, F., Cuxart, J., Delautier, G., Dauhut, T., Ducrocq, V., Filippi, J.-B., Gazen, D., Geoffroy, O., Gheusi, F., Honnert, R., Lafore, J.-P., Lebeaupin Brossier, C., Libois, Q., Lunet, T., Mari, C., Maric, T., Mascart, P., Mogé, M., Molinié, G., Nuissier, O., Pantillon, F., Peyrillé, P., Pergaud, J., Perraud, E., Pianezze, J., Redelsperger, J.-L., Ricard, D., Richard, E., Riette, S., Rodier, Q., Schoetter, R., Seyfried, L., Stein, J., Suhre, K., Taufour, M., Taufour, M., Thouron, O., Turner, S., Verrelle, A., Vié, B., Visentin, F., Vionnet, V., and Wautelet, P.: Overview of the Meso-NH model version 5.4 and its applications, Geosci. Model Dev. Discussions, pp. 1–66, https://doi.org/10.5194/gmd-2017-297, https://www.geosci-model-dev-discuss.net/gmd-2017-297/, 2018.

Lauer, A., Hendricks, J., Ackermann, I., Schell, B., Hass, H., and Metzger, S.: Simulating aerosol microphysics with the ECHAM/MADE GCM – Part I: Model description and comparison with observations, Atmos. Chem. Phys., 5, 3251–3276, https://doi.org/10.5194/acp-5-3251-2005, http://www.atmos-chem-phys.net/5/3251/2005/, 2005.

Lauer, A., Eyring, V., Hendricks, J., Joeckel, P., and Lohmann, U.: Global model simulations of the impact of ocean-going ships on aerosols, clouds, and the radiation budget, Atmos. Chem. Phys., 7, 5061–5079, https://doi.org/10.5194/acp-7-5061-2007, http://www.atmos-chem-phys.net/7/5061/2007/, 2007.

Lelieveld, J., Bruehl, C., Joeckel, P., Steil, B., Crutzen, P. J., Fischer, H., Giorgetta, M. A., Hoor, P., Lawrence, M. G., Sausen, R., and Tost, H.: Stratospheric dryness: model simulations and satellite observations, Atmos. Chem. Phys., 7, 1313–1332, https://doi.org/10.5194/acp-7-1313-2007, http://www.atmos-chem-phys.net/7/1313/2007/, 2007.

Liao, H.: Global impacts of gas-phase chemistry-aerosol interactions on direct radiative forcing by anthropogenic aerosols and ozone, J. Geophys. Res., 110, https://doi.org/10.1029/2005JD005907, http://doi.wiley.com/10.1029/2005JD005907, 2005.

Luo, C., Zender, C. S., Bian, H., and Metzger, S.: Role of ammonia chemistry and coarse mode aerosols in global climatological inorganic aerosol distributions, Atmos. Environ., 41, 2510–2533, https://doi.org/10.1016/j.atmosenv.2006.11.030, http://linkinghub.elsevier.com/retrieve/pii/S1352231006011666, 2007.

Manders, A., Ulft, B. v., Meijgaard, E. v., and Schaap, M.: Coupling of the air quality model LOTOS-EUROS to the climate model RACMO, in: Coupling of the air quality model LOTOS-EUROS to the climate model RACMO, Knowledge for Climate Programme Office, Utrecht, http://edepot.wur.nl/328070, oCLC: 911880649, 2011.

Metzger, S. and Lelieveld, J.: Reformulating atmospheric aerosol thermodynamics and hygroscopic growth into fog, haze and clouds, Atmos. Chem. Phys., 7, 3163–3193, https://doi.org/10.5194/acp-7-3163-2007, http://www.atmos-chem-phys.net/7/3163/2007/, 2007.

Metzger, S., Dentener, F., Krol, M., Jeuken, A., and Lelieveld, J.: Gas/aerosol partitioning: 2. Global modeling results, J. Geophys. Res., 107, https://doi.org/10.1029/2001JD001103, http://doi.wiley.com/10.1029/2001JD001103, 2002a.

Metzger, S., Dentener, F., Pandis, S., and Lelieveld, J.: Gas/aerosol partitioning: 1. A computationally efficient model, J. Geophys. Res., 107, https://doi.org/10.1029/2001JD001102, http://doi.wiley.com/10.1029/2001JD001102, 2002b.

Metzger, S., Mihalopoulos, N., and Lelieveld, J.: Importance of mineral cations and organics in gas-aerosol partitioning of reactive nitrogen compounds: case study based on MINOS results, Atmos. Chem. Phys., 6, 2549–2567, https://doi.org/10.5194/acp-6-2549-2006, http://www.atmos-chem-phys.net/6/2549/2006/, 2006.

Metzger, S., Steil, B., Xu, L., Penner, J. E., and Lelieveld, J.: New representation of water activity based on a single solute specific constant to parameterize the hygroscopic growth of aerosols in atmospheric models, Atmos. Chem. Phys., 12, 5429–5446, https://doi.org/10.5194/acp-12-5429-2012, http://www.atmos-chem-phys.net/12/5429/2012/, 2012.

Metzger, S., Abdelkader, M., Klingmueller, K., Steil, B., and Lelieveld, J.: Comparison of Metop PMAp Version 2 AOD Products using Model Data, Final Report EUMETSAT ITT 15/210839, EUMETSAT, Max Planck Institute for Chemistry, Department of Atmospheric Chemistry, http://bit.ly/2Epxf9b, 2016a.

Metzger, S., Steil, B., Abdelkader, M., Klingmueller, K., Xu, L., Penner, J. E., Fountoukis, C., Nenes, A., and Lelieveld, J.: Aerosol water parameterisation: a single parameter framework, Atmos. Chem. Phys., 16, 7213–7237, https://doi.org/10.5194/acp-16-7213-2016, http://www.atmos-chem-phys.net/16/7213/2016/, 2016b.

Monahan, E. C., Spiel, D. E., and Davidson, K. L.: A Model of Marine Aerosol Generation Via Whitecaps and Wave Disruption, in: Oceanic Whitecaps, edited by Monahan, E. C. and Niocaill, G. M., vol. 2, pp. 167–174, Springer Netherlands, Dordrecht, https://doi.org/10.1007/978-94-009-4668-2_16, http://www.springerlink.com/index/10.1007/978-94-009-4668-2_16, 1986.

Myhre, G., Grini, A., and Metzger, S.: Modelling of nitrate and ammonium-containing aerosols in presence of sea salt, Atmos. Chem. Phys., 6, 4809–4821, https://doi.org/10.5194/acp-6-4809-2006, http://www.atmos-chem-phys.net/6/4809/2006/, 2006.

Nenes, A., Pandis, S. N., and Pilinis, C.: ISORROPIA: A New Thermodynamic Equilibrium Model for Multiphase Multicomponent Inorganic Aerosols, Aquat. Geochem., 4, 123–152, 1998.

Nguyen, T. K. V., Ghate, V. P., and Carlton, A. G.: Reconciling satellite aerosol optical thickness and surface fine particle mass through aerosol liquid water: ALW AND AOT, Geophys. Res. Letters, 43, 11,903–11,912, https://doi.org/10.1002/2016GL070994, http://doi.wiley.com/10.1002/2016GL070994, 2016.

Pozzer, A., Joeckel, P., Sander, R., Williams, J., Ganzeveld, L., and Lelieveld, J.: Technical Note: The MESSy-submodel AIRSEA calculating the air-sea exchange of chemical species, Atmos. Chem. Phys., 6, 5435–5444, https://doi.org/10.5194/acp-6-5435-2006, http://www.atmos-chem-phys.net/6/5435/2006/, 2006.

Pozzer, A., de Meij, A., Pringle, K. J., Tost, H., Doering, U. M., van Aardenne, J., and Lelieveld, J.: Distributions and regional budgets of aerosols and their precursors simulated with the EMAC chemistry-climate model, Atmos. Chem. Phys., 12, 961–987, https://doi.org/10.5194/acp-12-961-2012, http://www.atmos-chem-phys.net/12/961/2012/, 2012.

Pozzer, A., de Meij, A., Yoon, J., Tost, H., Georgoulias, A. K., and Astitha, M.: AOD trends during 2001–2010 from observations and model simulations, Atmos. Chem. Phys., 15, 5521–5535, https://doi.org/10.5194/acp-15-5521-2015, http://www.atmos-chem-phys.net/15/5521/2015/, 2015.

Pozzer, A., Tsimpidi, A. P., Karydis, V. A., de Meij, A., and Lelieveld, J.: Impact of agricultural emission reductions on fine-particulate matter and public health, Atmos. Chem. Phys., 17, 12 813–12 826, https://doi.org/10.5194/acp-17-12813-2017, https://www.atmos-chem-phys.net/17/12813/2017/, 2017.

Pringle, K. J., Tost, H., Message, S., Steil, B., Giannadaki, D., Nenes, A., Fountoukis, C., Stier, P., Vignati, E., and Lelieveld, J.: Description and evaluation of GMXe: a new aerosol submodel for global simulations (v1), Geosci. Model Dev., 3, 391–412, https://doi.org/10.5194/gmd-3-391-2010, http://www.geosci-model-dev.net/3/391/2010/, 2010a.

Pringle, K. J., Tost, H., Metzger, S., Steil, B., Giannadaki, D., Nenes, A., Fountoukis, C., Stier, P., Vignati, E., and Lelieveld, J.: Corrigendum to "Description and evaluation of GMXe: a new aerosol submodel for global simulations (v1)" published in Geosci. Model Dev., 3, 391–412, 2010, Geosci. Model Dev., 3, 413–413, https://doi.org/10.5194/gmd-3-413-2010, http://www.geosci-model-dev.net/3/413/2010/, 2010b.

Sander, R., Kerkweg, A., Joeckel, P., and Lelieveld, J.: Technical note: The new comprehensive atmospheric chemistry module MECCA, Atmos. Chem. Phys., 5, 445–450, https://doi.org/10.5194/acp-5-445-2005, http://www.atmos-chem-phys.net/5/445/2005/, 2005.

Saxena, P., Belle Hudischewskyj, A., Seigneur, C., and Seinfeld, J. H.: A comparative study of equilibrium approaches to the chemical characterization of secondary aerosols, Atmos. Environ. (1967), 20, 1471–1483, https://doi.org/10.1016/0004-6981(86)90019-3, http://linkinghub.elsevier.com/retrieve/pii/0004698186900193, 1986.

Schell, B., Ackermann, I. J., Hass, H., Binkowski, F. S., and Ebel, A.: Modeling the formation of secondary organic aerosol within a comprehensive air quality model system, J. Geophys. Res.: Atmospheres, 106, 28 275–28 293, https://doi.org/10.1029/2001JD000384, http://doi.wiley.com/10.1029/2001JD000384, 2001.

Simpson, D., Fagerli, H., Jonson, J. E., Tsyro, S., Wind, P., and Tuovinen, J.-P.: Transboundary Acidification, Eutrophication and Ground Level Ozone in Europe. PART I Unified EMEP Model Description., EMEP Status Report 2003 EMEP Report 1/2003, Norwegian Meteorological Institute, http://www.emep.int/publ/reports/2003/emep_report_1_part1_2003.pdf, 2003.

Simpson, D., Benedictow, A., Berge, H., Bergstroem, R., Emberson, L. D., Fagerli, H., Flechard, C. R., Hayman, G. D., Gauss, M., Jonson, J. E., Jenkin, M. E., Nyíri, A., Richter, C., Semeena, V. S., Tsyro, S., Tuovinen, J.-P., Valdebenito, A., and Wind, P.: The EMEP MSC-W chemical transport model – technical description, Atmos. Chem. Phys., 12, 7825–7865, https://doi.org/10.5194/acp-12-7825-2012, http://www.atmos-chem-phys.net/12/7825/2012/, 2012.

Tost, H., Joeckel, P., Kerkweg, A., Sander, R., and Lelieveld, J.: Technical note: A new comprehensive SCAVenging submodel for global atmospheric chemistry modelling, Atmos. Chem. Phys., 6, 565–574, https://doi.org/10.5194/acp-6-565-2006, http://www.atmos-chem-phys.net/6/565/2006/, 2006a.

Tost, H., Joeckel, P., and Lelieveld, J.: Influence of different convection parameterisations in a GCM, Atmos. Chem. Phys., 6, 5475–5493, https://doi.org/10.5194/acp-6-5475-2006, http://www.atmos-chem-phys.net/6/5475/2006/, 2006b.

Tost, H., Joeckel, P., and Lelieveld, J.: Lightning and convection parameterisations – uncertainties in global modelling, Atmos. Chem. Phys., 7, 4553–4568, https://doi.org/10.5194/acp-7-4553-2007, http://www.atmos-chem-phys.net/7/4553/2007/, 2007.

Trebs, I., Metzger, S., Meixner, F. X., Helas, G., Hoffer, A., Rudich, Y., Falkovich, A. H., Moura, M. A. L., da Silva Jr., R. S., Artaxo, P., Slanina, J., and Andreae, M. O.: The NH_4^+ -NO_3^- -Cl^- -SO_4^{2-} -H_2O aerosol system and its gas phase precursors at a pasture site in the Ama-

zon Basin: How relevant are mineral cations and soluble organic acids?, J. Geophys. Res., 110, https://doi.org/10.1029/2004JD005478, http://doi.wiley.com/10.1029/2004JD005478, 2005.

Tsigaridis, K., Krol, M., Dentener, F. J., Balkanski, Y., Lathière, J., Metzger, S., Hauglustaine, D. A., and Kanakidou, M.: Change in global aerosol composition since preindustrial times, Atmos. Chem. Phys., 6, 5143–5162, https://doi.org/10.5194/acp-6-5143-2006, http://www.atmos-chem-phys.net/6/5143/2006/, 2006.

Tørseth, K., Aas, W., Breivik, K., Fjæraa, A. M., Fiebig, M., Hjellbrekke, A. G., Lund Myhre, C., Solberg, S., and Yttri, K. E.: Introduction to the European Monitoring and Evaluation Programme (EMEP) and observed atmospheric composition change during 1972–2009, Atmos. Chem. Phys., 12, 5447–5481, https://doi.org/10.5194/acp-12-5447-2012, http://www.atmos-chem-phys.net/12/5447/2012/, 2012.

Van Meijgaard, E. and KNMI.: The KNMI regional atmospheric climate model RACMO version 2.1., Koninklijk Nederlands Meteorologisch Instituut, De Bilt, 2008.

von Kuhlmann, R., Lawrence, M. G., Crutzen, P. J., and Rasch, P. J.: A model for studies of tropospheric ozone and nonmethane hydrocarbons: Model description and ozone results: MATCH-MPIC DESCRIPTION AND OZONE RESULTS, J. Geophys. Res.: Atmospheres, 108, n/a–n/a, https://doi.org/10.1029/2002JD002893, http://doi.wiley.com/10.1029/2002JD002893, 2003.

Zhang, Y., Sartelet, K., Wu, S.-Y., and Seigneur, C.: Application of WRF/Chem-MADRID and WRF/Polyphemus in Europe – Part 1: Model description, evaluation of meteorological predictions, and aerosol–meteorology interactions, Atmos. Chem. Phys., 13, 6807–6843, https://doi.org/10.5194/acp-13-6807-2013, http://www.atmos-chem-phys.net/13/6807/2013/, 2013.

Table 1. Modeling systems that provide an option to use EQSAM and/or ISORROPIA. References are given for certain model versions: EQSAM_v03d (EQ1, Metzger et al. (2002b)), EQSAM2 (EQ2, Metzger et al. (2006)), EQSAM3 (EQ3, Metzger and Lelieveld (2007)), EQSAM4clim (EQ4c, Metzger et al. (2016b)) and/or ISORROPIA-I (ISO1, Nenes et al. (1998)), ISORROPIA-II (ISO2, Fountoukis and Nenes (2007)). URL: CAMx – http://www.camx.com; CHIMERE – http://www.lmd.polytechnique.fr/chimere/; EMAC – http://www.messy-interface.org/; EMEP – http://www.emep.int; GEOS – https://gmao.gsfc.nasa.gov/GEOS; LOTOS-EUROS – https://lotos-euros.tno.nl; Meso-NH – http://mesonh.aero.obs-mip.fr/; NASA GISS – https://www.giss.nasa.gov; POLYPHEMUS – http://cerea.enpc.fr/polyphemus; RACMO – https://www.knmi.nl/; WRF – https://www.mmm.ucar.edu/weather-research-and-forecasting-model.

Modeling System	Model	Reference
CAMx	ISO1	Koo et al. (2009), CAMx User's Guide Version 6.40 (Environ, 2016)
CHIMERE	EQ1 / ISO1	Bessagnet et al. (2004), de Meij, A. (2009)
EMAC/GMXe	EQ4c	Metzger et al. (2016b), Metzger et al. (2016a), Abdelkader et al. (2017)
EMAC/GMXe	ISO2	de Meij et al. (2012), Karydis et al. (2016), Pozzer et al. (2017)
EMAC/MADE3	EQ1	Lauer et al. (2005), Kaiser et al. (2014)
EMEP	EQ1 / ISO1	Simpson et al. (2003), Simpson et al. (2012)
GEOS-5	EQ1	Darmenov et al. (2016), https://bit.ly/2FaO7E1
Meso-NH	EQ1 / ISO1	Lac et al. (2018), General docu of Meso-NH v5.1 (https://bit.ly/2pJDe2c)
NASA/GISS	EQ1 / ISO2	Bauer et al. (2007a), Bauer et al. (2007b), Bian et al. (2017)
WRF/POLYPHEMUS	EQ1 / ISO2	Zhang et al. (2013); Polyphemus 1.6 User's Guide https://bit.ly/2DVNpG4
RACMO-LOTOS-EUROS	EQ1	Van Meijgaard and KNMI. (2008), Manders et al. (2011)
TM3/TM5	EQ1 / ISO2	Metzger et al. (2002a), Dentener et al. (2002), de Meij et al. (2006)
CAMx	EQ4c	Under evaluation (Koo et al., 2018), CAMx User's Guide Version 6.45
EMEP	EQ4c	Implementation in progress (inclusion foreseen in Report 2018)

Table 2. Parameters for the different chemical aging levels of bulk species shown in Table 4 (Sec. 4.2). ν_{bulk} $[-]$ denotes the bulk water uptake coefficient, RHD_{bulk} [%] the bulk water uptake threshold and MF_{bulk} [%] the mass fraction used for chemical aging of the bulk aerosol species. The main reagent that is assumed to determine the chemical aging (through implicit coating and water uptake) is included below the bulk species. The values have been empirically determined by numerous model applications and a very comprehensive model evaluation by the constraint to yield the best agreement of our EMAC version with independent model results and various observations. Key results of this evaluation cycle are shown in Sec. 3, additional results will be presented separately.

Bulk compound with main reagent	BC NH_4NO_3 | NH_4HSO_4	OC $(NH_4)_2SO_4$ | NH_4HSO_4	DU $Ca(Cl)_2$ | $Ca(NO_3)_2$	SS $NaCl$ | $NaCl$
Aging case	50 | 90%	50 | 90%	50 | 90%	50 | 90%
ν_{bulk}	1.051 | 1.254	1.275 | 1.254	2.025 | 1.586	1.358 | 1.358
MF_{bulk}	50 | 90	50 | 40	75 | 90	100 | 50
RHD_{bulk}	60 | 40	80 | 90	28 | 49	50 | 75

Table 3. EMAC tracer statistics for the year 2005 and 189 stations based on 5 hourly model output. Simulations based on ISORROPIA II (ISO2) and EQSAM4clim (EQ4c) (identical EMAC setup).

	STATION MEAN		RMSE	CORR	MBE
	ISO2	EQ4c	–	–	–
PM	58.05 ± 193.45	57.23 ± 193.03	3.64	1.00	-0.82
DU	41.91 ± 192.84	41.75 ± 192.34	3.41	1.00	-0.17
SS	6.83 ± 8.47	6.37 ± 7.78	0.93	1.00	-0.45
OC	2.32 ± 1.94	2.33 ± 1.94	0.07	1.00	0.01
BC	0.45 ± 0.56	0.45 ± 0.56	0.01	1.00	-0.00
H_2O	14.48 ± 13.71	13.53 ± 13.07	2.32	0.99	-0.96
NO_3^-	1.26 ± 1.02	1.16 ± 0.95	0.30	0.96	-0.10
SO_4^{2-}	2.25 ± 1.53	2.40 ± 1.66	0.32	0.99	0.15
H_2SO_4	0.02 ± 0.03	0.02 ± 0.03	0.00	1.00	-0.00
$HSO4^-$	0.22 ± 0.47	0.12 ± 0.27	0.24	0.99	-0.10
Ca^{2+}	2.25 ± 10.28	2.24 ± 10.26	0.18	1.00	-0.01
Mg^{2+}	0.19 ± 0.24	0.18 ± 0.22	0.03	1.00	-0.01
NH_4^+	0.85 ± 0.71	0.81 ± 0.69	0.09	0.99	-0.04
Na^+	0.66 ± 0.81	0.62 ± 0.75	0.08	1.00	-0.04
Cl^-	0.64 ± 0.90	0.56 ± 0.83	0.15	0.99	-0.08
K^+	0.19 ± 0.12	0.19 ± 0.12	0.01	1.00	-0.00
H^+	0.02 ± 0.02	0.02 ± 0.02	0.01	0.93	0.00
OH^-	0.06 ± 0.09	0.06 ± 0.09	0.02	0.97	0.00
NO	0.63 ± 1.09	0.62 ± 1.07	0.09	1.00	-0.00
NO_2	6.00 ± 6.70	5.98 ± 6.66	0.18	1.00	-0.02
SO_2	3.53 ± 3.28	3.50 ± 3.25	0.13	1.00	-0.03
HNO_3	1.64 ± 2.01	1.69 ± 2.05	0.21	1.00	0.05
HCl	0.20 ± 0.20	0.21 ± 0.20	0.08	0.93	0.01
O_3	56.61 ± 19.34	56.41 ± 19.29	0.69	1.00	-0.20
RWETAER	1.95 ± 0.17	1.95 ± 0.17	0.03	0.99	0.00
RDRYAER	1.75 ± 0.07	1.75 ± 0.06	0.01	0.98	0.00
AERNUMB	260.36 ± 130.37	264.54 ± 132.55	21.72	0.99	4.18
RH	69.16 ± 20.81	69.20 ± 20.79	0.69	1.00	0.04
T	18.94 ± 28.84	18.95 ± 28.83	5.11	0.98	0.01

Table 4. Sensitivity runs with different levels of chemical aging of bulk species as defined in Sec. 4.2 and Table 2. Note that the key difference between "no aging" and "aging" case is the water uptake of primary particles. It is only considered for the latter case (being based on Sec. 2.4 and 2.5). All cases include the GMXe coating processes (Sec. 2.2) through condensation of gases such as hydrochloric acid, nitric acid, sulfuric acid and ammonia on insoluble particles (mineral dust, black and organic carbon). Additionally, in all cases particles can mix through coagulation, and the formation of semi-volatile salt-compounds such as ammonium nitrate and ammonium chloride, and gas-aerosol partitioning including water uptake (Sec. 2.3), is always applied for compounds in the soluble modes.

Case	Simulation	Option1	Option2	Option3	Application
	"label"	aerosol water	bulk aging	hysteresis effect	Section
1	"no aging"	yes	no	no	Sec. 4.1 + S1.3
2	"no water"	no	no	no	Sec. 2.5
3	50% aging	yes	50%	yes	Sec. 4.2 + 3.3
4	"90% aging"	yes	90%	yes	Sec. 2.5

Table 5. CPU times. EMAC @ 96 CPU cores, Cy-Tera (http://web.cytera.cyi.ac.cy/).

Simulation	Memory [Gb/node]	CPU-time [h/node]	Wall-time [h]
A – ISORROPIAII	5.713064	173:49:49	14:31:26
B – EQSAM4clim	5.751476	158:53:35	13:16:42
C – EQSAM4clim	5.756064	158:08:04	13:12:58
D – none of both	5.738376	153:11:01	12:48:10
A_0 – ISORROPIAII	5.748988	172:33:56	14:25:05
B_0 – EQSAM4clim	5.744580	152:24:34	12:44:16

Table A1. List of names and abbreviations.

Abbreviation	Name
AERONET	AErosol RObotic NETwork (http://aeronet.gsfc.nasa.gov)
AOD	Aerosol Optical Depth (https://earthobservatory.nasa.gov/GlobalMaps/view.php?d1=MODAL2_M_AER_OD)
CPU	Computational Performance Unit (https://en.wikipedia.org/wiki/Central_processing_unit)
Cy-Tera	The Cyprus Institute high performance computing system (http://web.cytera.cyi.ac.cy/)
DKRZ	The German Climate Computing Center high performance computing system (https://www.dkrz.de)
EMAC	ECHAM5/MESSy Atmospheric Chemistry-climate model (Joeckel et al. (2005), Joeckel et al. (2010))
EQSAM4clim	Equilibrium Simplified Aerosol Model (Version 4) for Climate Simulations (Metzger et al., 2016b)
GMXe	Aerosol microphysics model, Global Modal-aerosol eXtension (Pringle et al., 2010a)
ISORROPIA II	Equilibrium Aerosol Model Nenes et al. (1998), Fountoukis and Nenes (2007)
MODIS	Satellite observations (http://modis-atmos.gsfc.nasa.gov/)
MISR	Global satellite data (https://giovanni.gsfc.nasa.gov/giovanni/)
SCALASCA	performance measuring software tool (http://www.scalasca.org/, https://bit.ly/2GF5IoB)

AERONET/EMEP stations
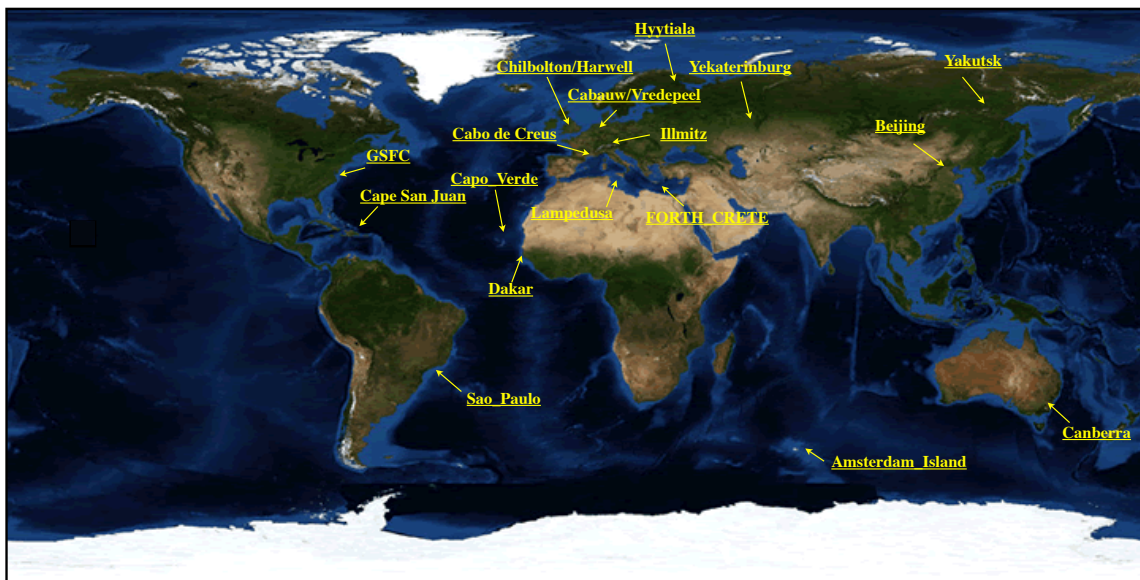
AERONET - http://aeronet.gsfc.nasa.gov/cgi-bin/type_piece_of_map_opera_v2_new   EMEP - http://ebas.nilu.no/default.aspx

Amsterdam_Island (37S,77E)	Sao_Paulo (23S,46W)	Dakar (14N,16W)	Cabauw (51N,4E)	Lampedusa (35N,12E)	Yekaterinburg (57N,59E)	Beijing (39N,116E)
GSFC (38N,76W)	Cape_San_Juan (18N,65W)	Capo_Verde (16N,22W)	Chilbolton (51N,1W)	FORTH_CRETE (35N,25E)	Yakutsk (61N,129E)	Canberra (35S,149E)
EMEP	Cabo de Creus (42N,3E)	Vredepeel (51N,4E)	Harwell (51N,1W)	Cabauw (51N,4E)	Illmitz (48N,16E)	Hyytiala (61N,24E)

Figure 1. Locations of selected AERONET and EMEP stations used in this EMAC evaluation study. The corresponding regions are shown in Fig. S1 (Supplement).
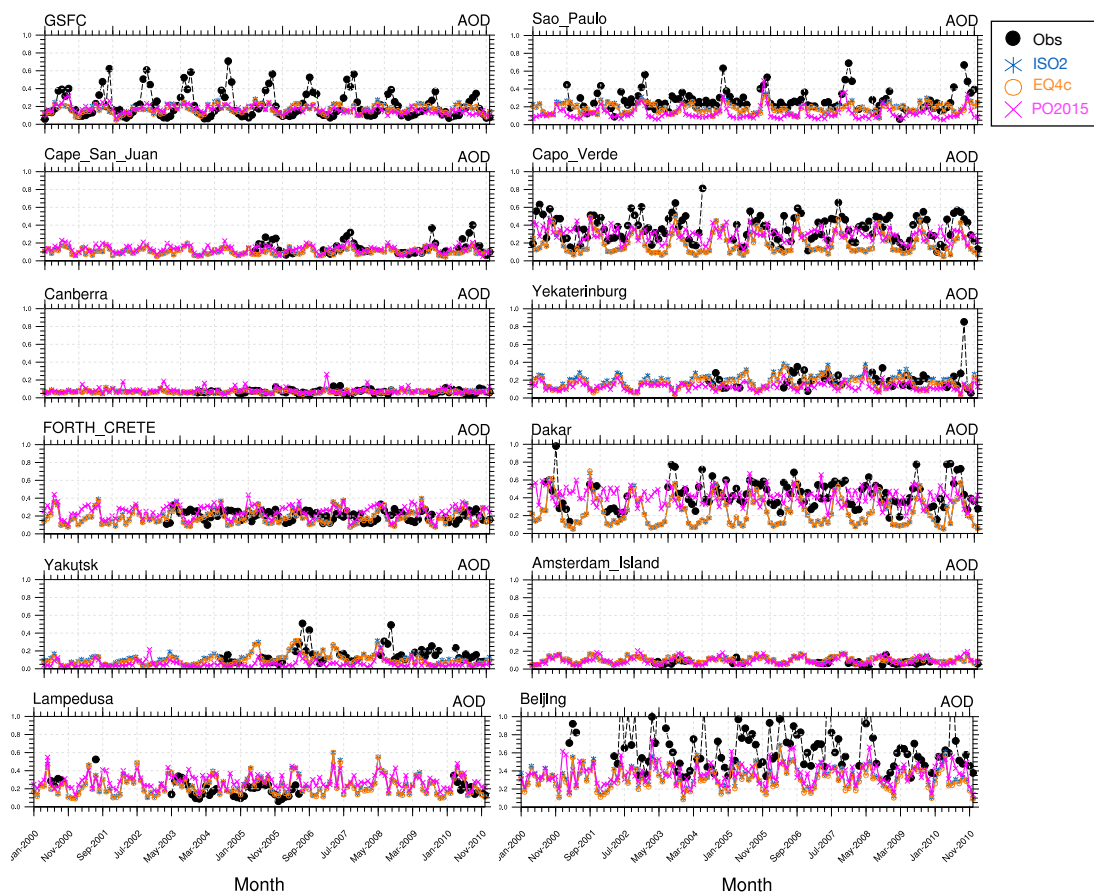
Figure 2. Selected AOD time-series for 2000-2010 (monthly means) for the stations shown in Fig. 1, representing all regions of Fig. S1. EMAC results based on ISORROPIA II (ISO2), EQSAM4clim (EQ4c) versus AERONET observations (black circles) and Pozzer et al. (2015) (PO2015). Additionally, scatter plots (Figs. S2– S4) are shown in the Supplement for 537 AERONET stations (Fig. S1).
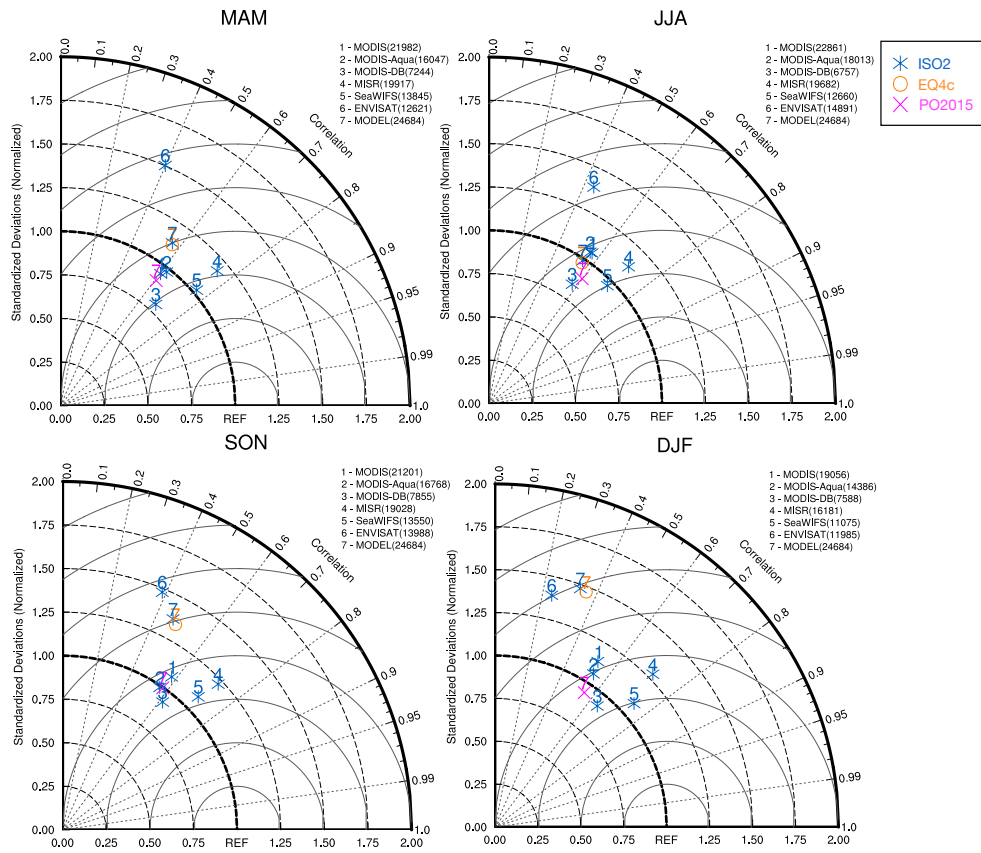
Figure 3. Taylor diagram for satellite and model AOD (2000-2010 mean). MODIS (1), MODIS-Aqua (2), MODIS-deep blue (3), MISR (4), SeaWIFS (5), ENVISAT (6) and models (7), i.e., ISORROPIA II (ISO2), EQSAM4clim (EQ4c), Pozzer et al. (2015) (PO2015), versus AERONET observations for the four seasons: spring (MAM), summer (JJA), autumn (SON), winter (DJF). The number of observational points used in the seasonal analysis are shown in parenthesis.
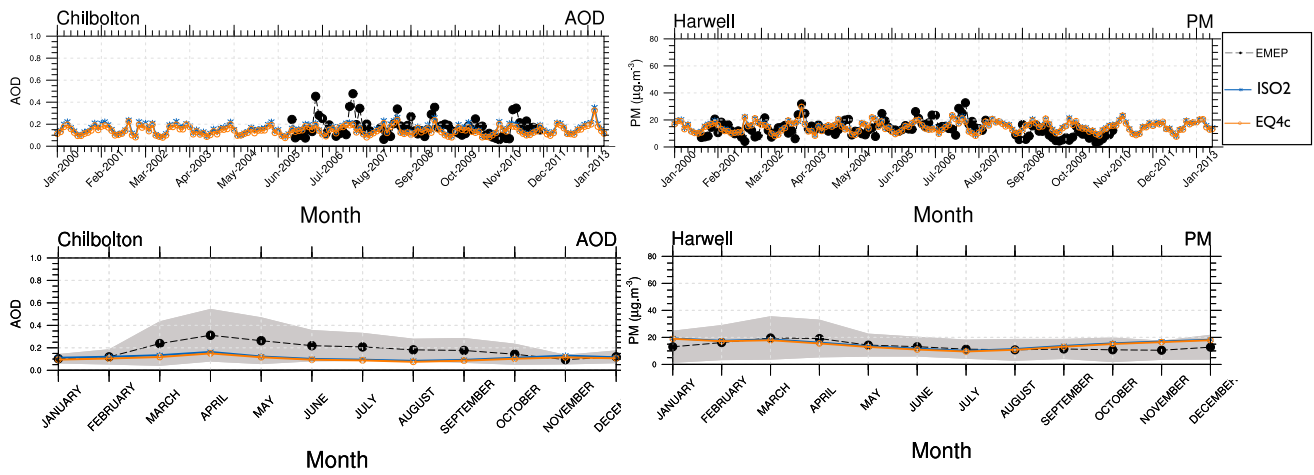
Figure 4. AOD and PM time-series for 2000-2013 (monthly means): ISORROPIA II (ISO2) and EQSAM4clim (EQ4c) versus AERONET and EMEP observations (upper panels). The lower panels show the corresponding climatological year for the AOD and PM (14 years average). The two stations Harwell and Chilbolton (United Kingdom) lie well within one model grid box (51N,1W).
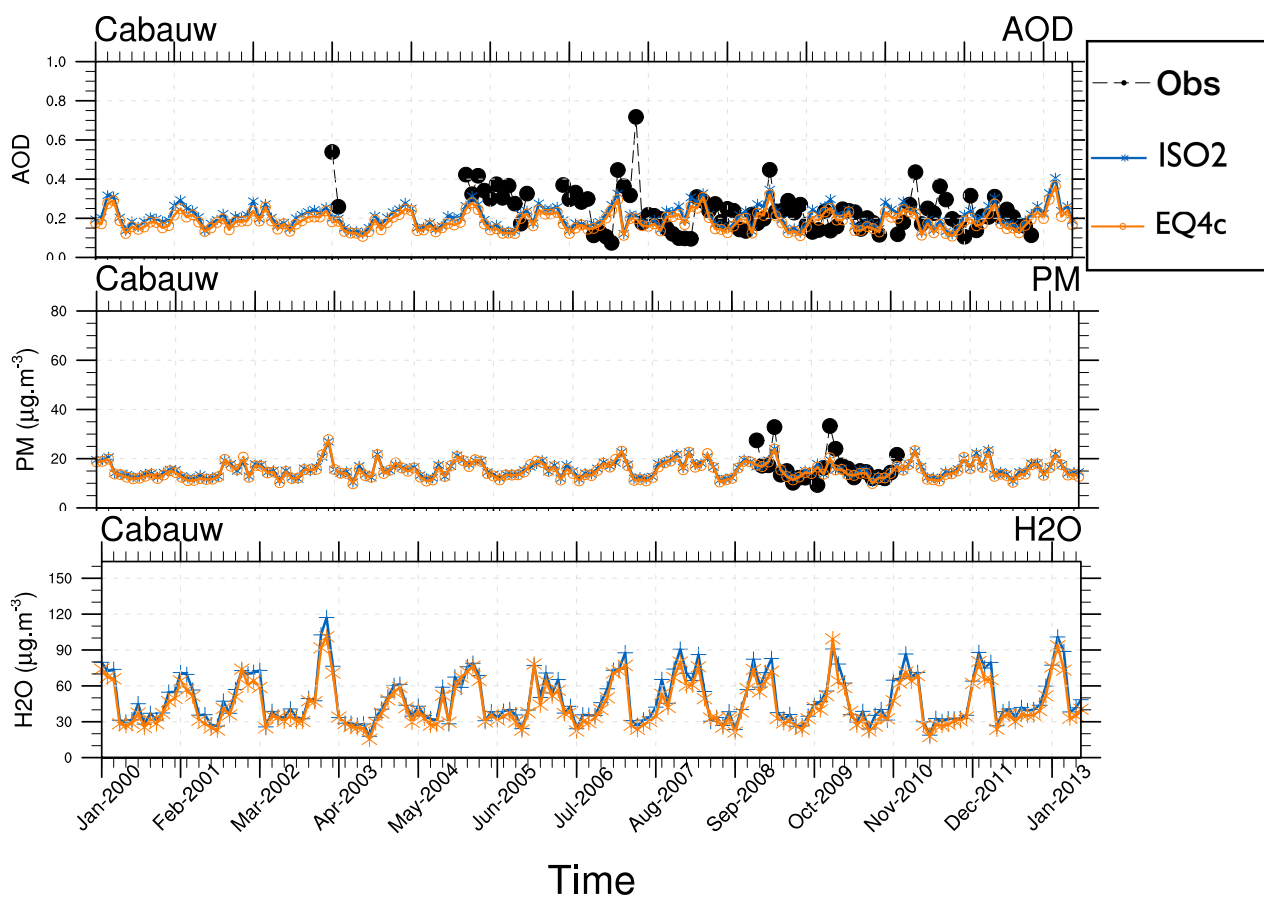
Figure 5. AOD (top), total (liquids and solids) particulate matter (PM) (middle), aerosol associated water (bottom) at EMEP station Cabauw for 2000-2013 (monthly means): ISORROPIA II (ISO2), EQSAM4clim (EQ4c), AERONET observations (black circles). Available observations are shown. Additionally, various size-resolved aerosol properties are shown in the Supplement (Figure S5).
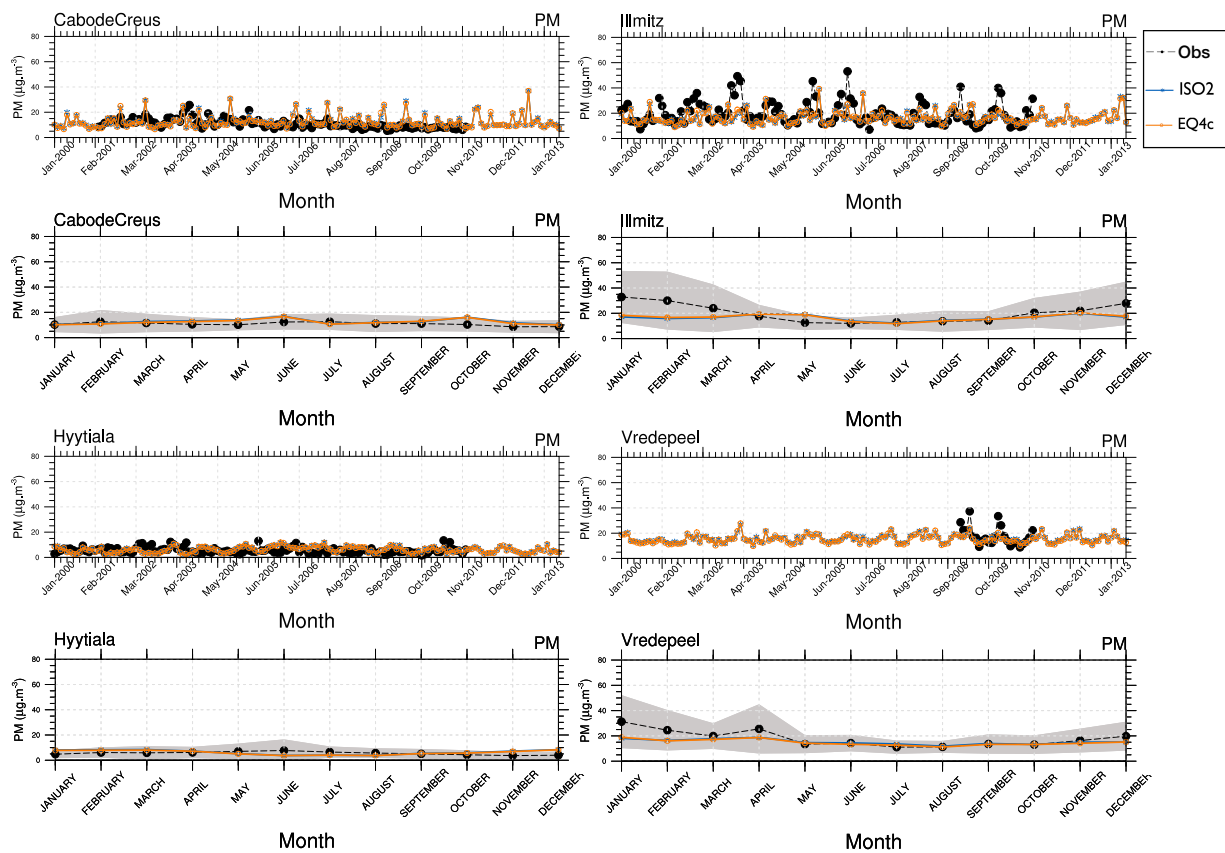
Figure 6. Aerosol mass (PM) time-series for 2000-2013 (monthly means): ISORROPIA II (ISO2) and EQSAM4clim (EQ4c) versus EMEP stations, which have long-term observations (top panels). The corresponding climatological year (14 years average) is shown below each time-series.
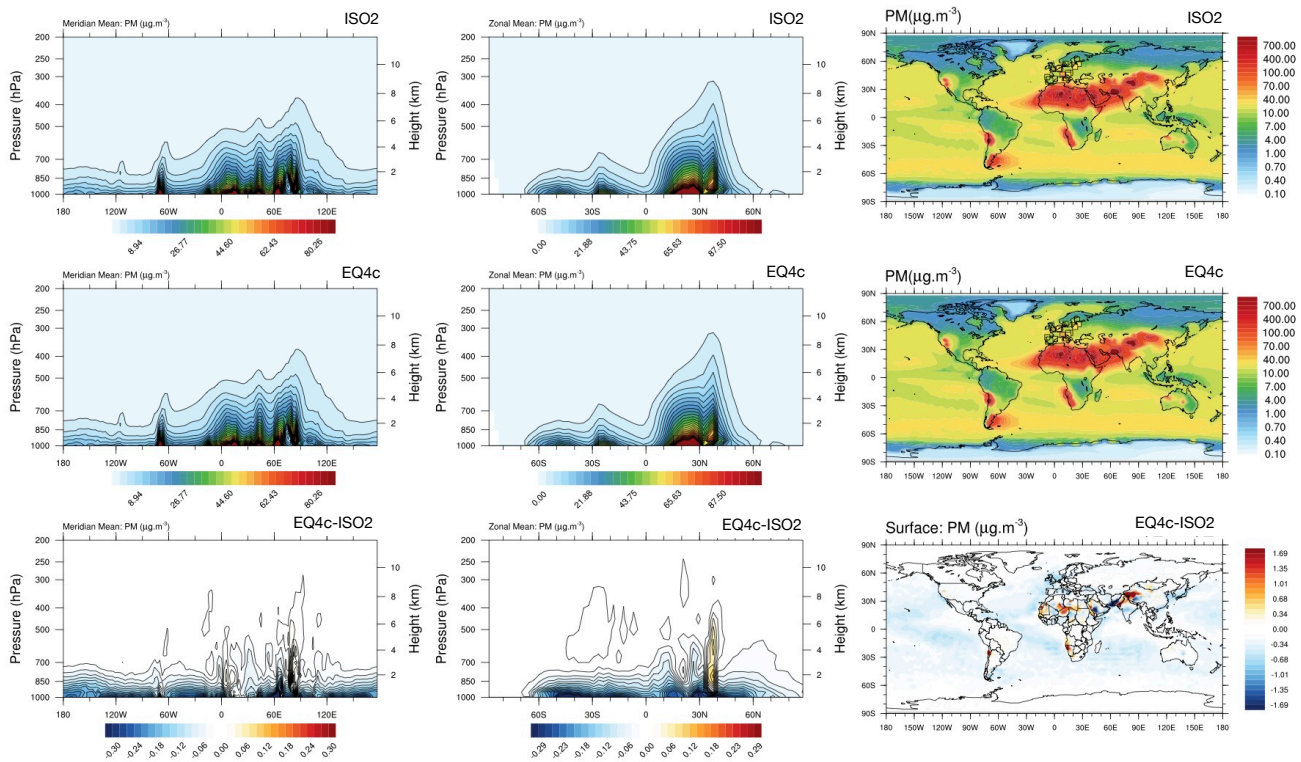
Figure 7. Global aerosol distributions of the total (liquids and solids) particulate matter: meridional mean (left column), zonal mean (middle column), atmospheric burden (right column). The EMAC results shown are based on ISORROPIA II (ISO2, top row), EQSAM4clim (EQ4c, middle row), and the corresponding difference between both simulations (EQ4c minus ISO2, bottom row).
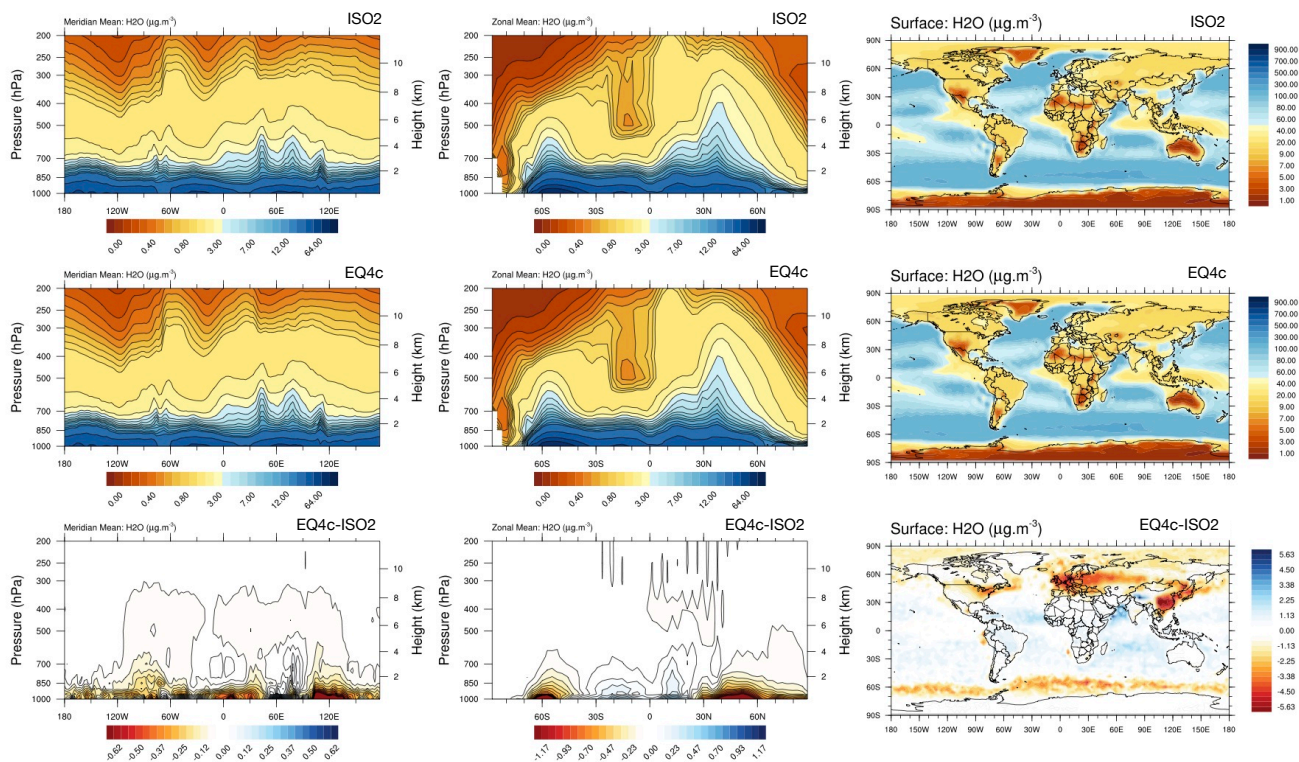
Figure 8. Fig. 7 continued for EMAC aerosol associated water (2000-2013 mean). Please note the inversion of the color scale (compared to Fig. 7).
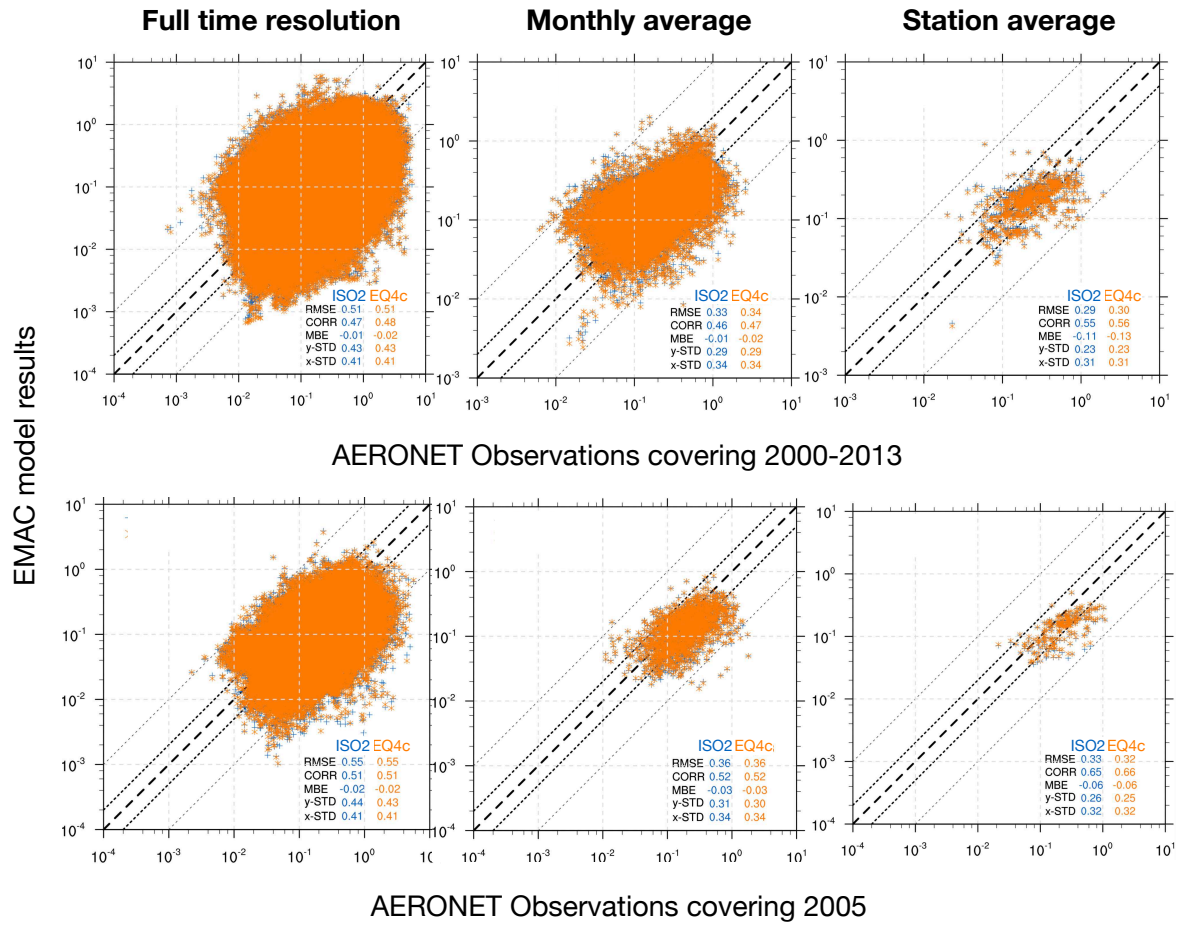
Figure 9. EMAC AOD versus AERONET observations for the period 2000-2013 (top) and the year 2005 (bottom). Different time averages are shown for the results of ISORROPIA II (ISO2) and EQSAM4clim (EQ4c) based on 537 AERONET station locations (Figure S1 of the Supplement).
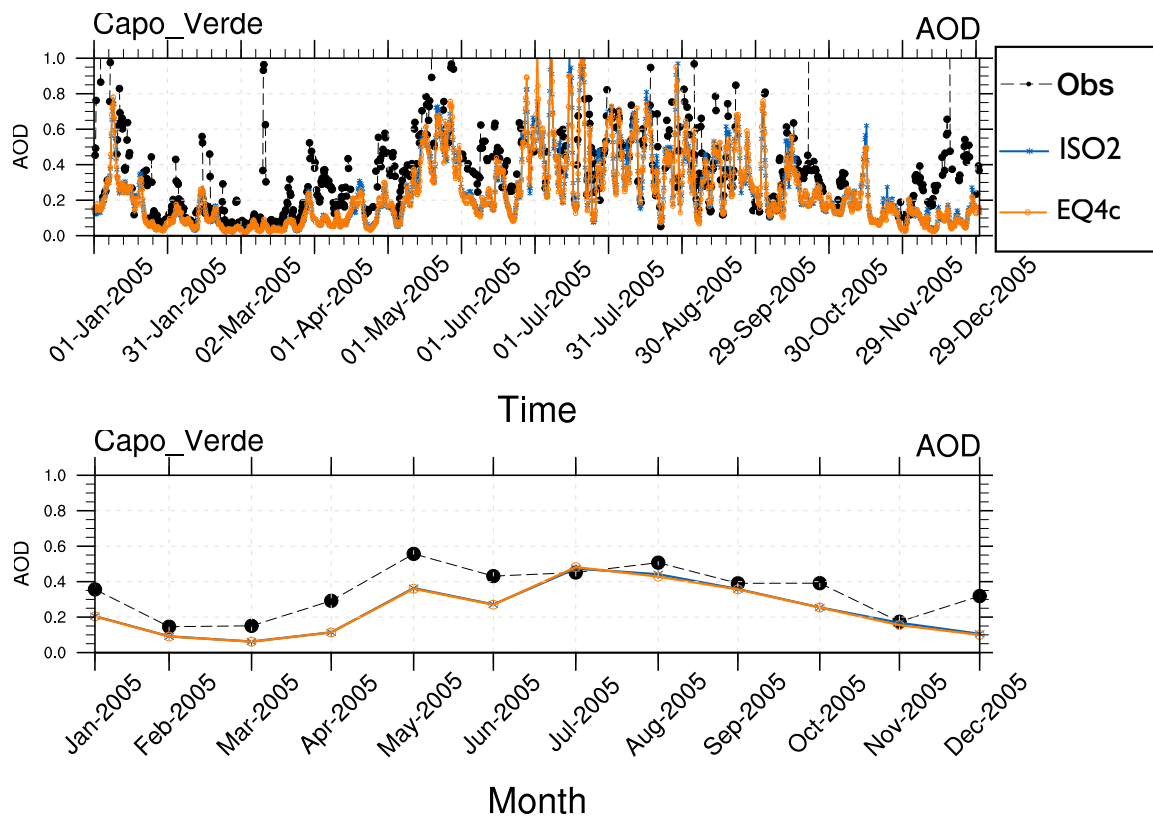
Figure 10. EMAC AOD results versus AERONET observation (Obs) at Capo Verde (year 2005); (top) 5 hourly means, (bottom) monthly means; EQSAM4clim (EQ4c) and ISORROPIA II (ISO2).
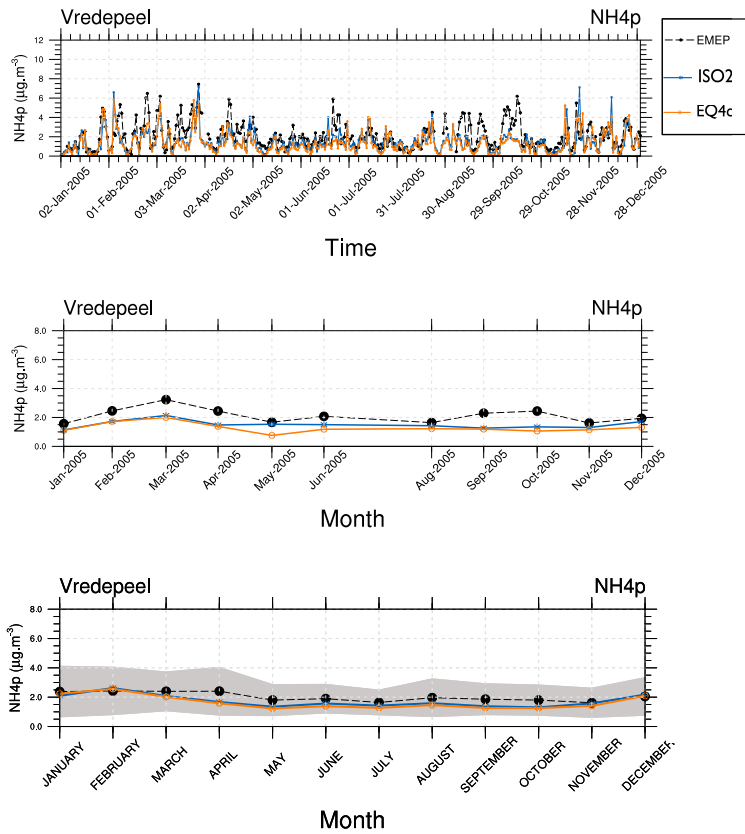
Figure 11. Total (liquids and solids) particulate ammonium (NH$_4^+$) at EMEP site Vredepeel for the year 2005. Daily means (top), monthly means (middle), climatological year based on the 14 years monthly mean (bottom). ISORROPIA II (ISO2), EQSAM4clim (EQ4c) versus observations (EMEP).

AOD (550nm) - 2005 (annual mean)
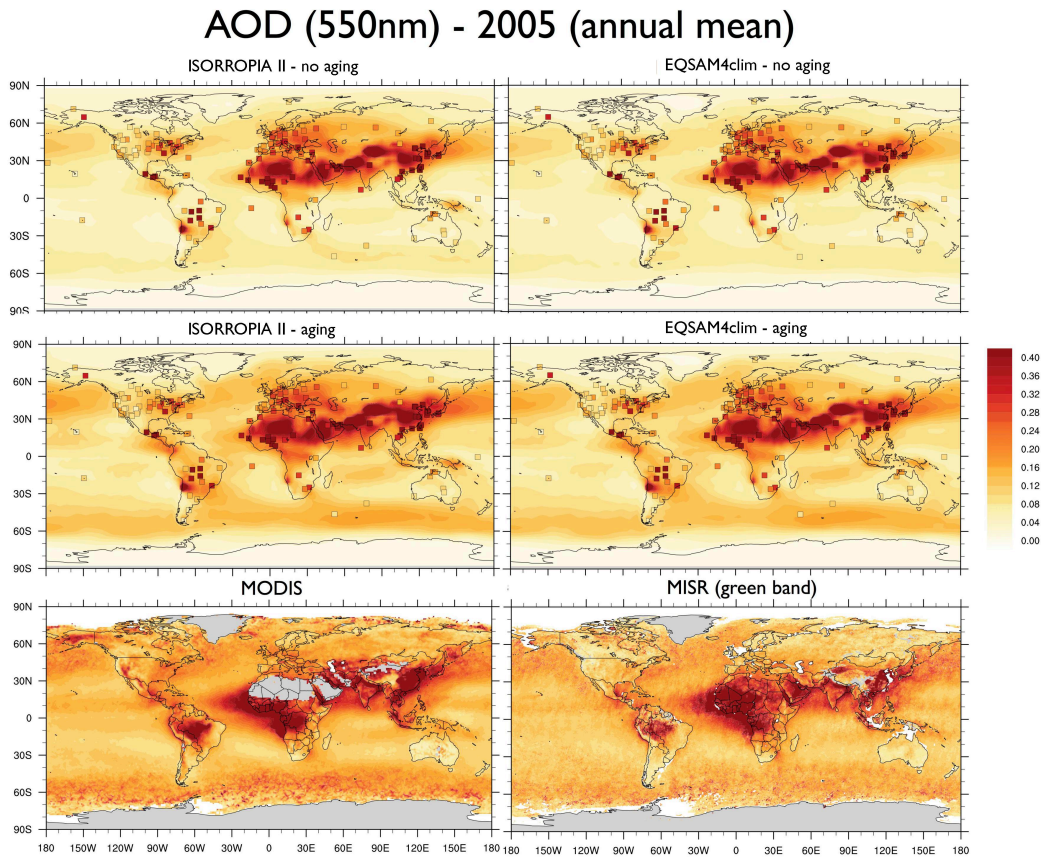
Figure 12. EMAC model AOD results for the year 2005 (annual mean) based on ISORROPIA II (left) and EQSAM4clim (right). Upper row: "$no\,aging$", middle row: "$aging$" case. AERONET ground station observations are included as squares (same color scale). Lower row: Satellite observations by MODIS (left) and MISR (right) (550nm, annual mean 2005). MODIS monitors the ambient AOD from space and provides data over the oceans and, except desserts, also over continents (http://modis-atmos.gsfc.nasa.gov/). The MISR aerosol product is available globally (products can be obtained from http://disc.sci.gsfc.nasa.gov/giovanni).
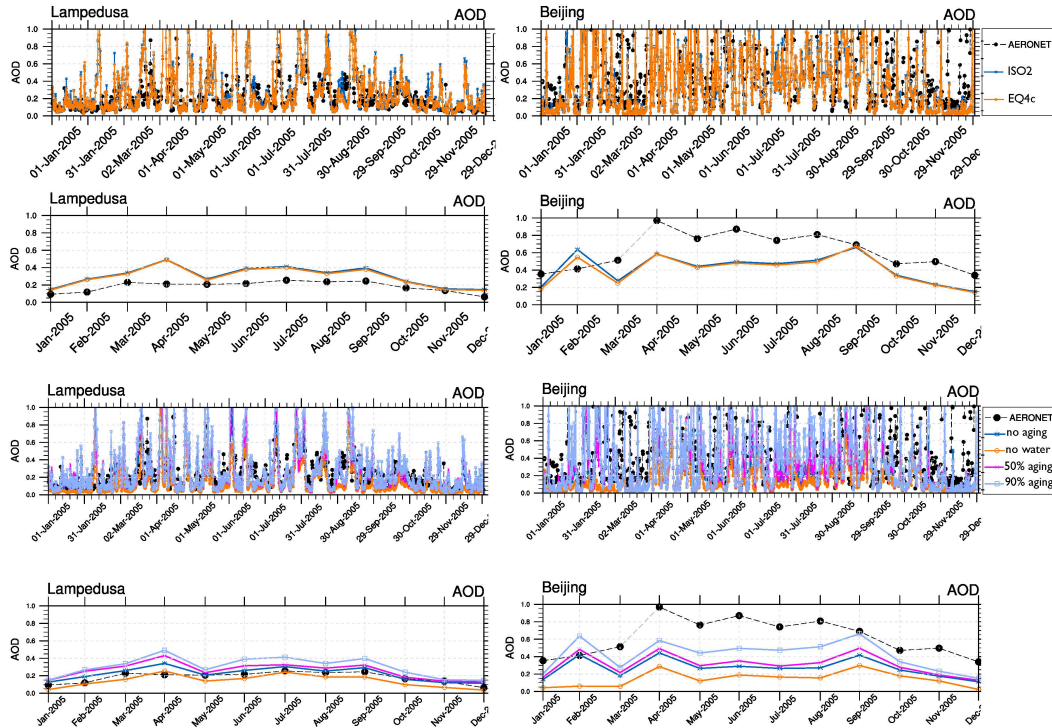
Figure 13. EMAC AOD results versus AERONET observations at Lampedusa and Beijing (shown in Fig. 2) for the year 2005. First and third row: 5 hourly means; 2nd and 3rd row: monthly means. Upper two rows show EQSAM4clim (EQ4c) and ISORROPIA II (ISO2), lowest two rows sensitivity of EMAC AOD to different water assumptions considering different EMAC setups; "no aging" (blue stars), "no water" without aerosol water (orange circles), "50% aging" (pink crosses), "90% aging" (light blue squares); see Table 4 and Table 2 (Sec. 4.2). The sensitivity is based on ISORROPIA II.
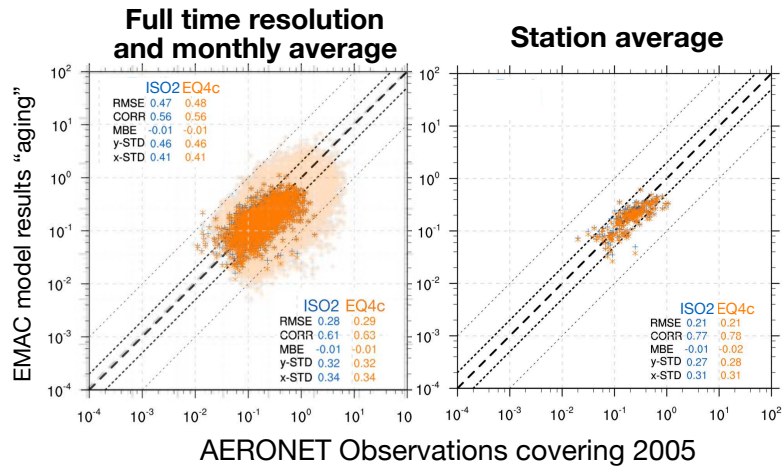
Figure 14. EMAC AOD based on the "aging" set-up versus AERONET observations for the year 2005, complementing Fig. 9. Different time averages (full time resolution in light colors with statistics in the upper left corner) are shown for the results of ISORROPIA II (ISO2) and EQSAM4clim (EQ4c) based on 537 AERONET station locations (shown in Figure S1 of the Supplement).

AOD (550nm) - 2005 (annual mean)
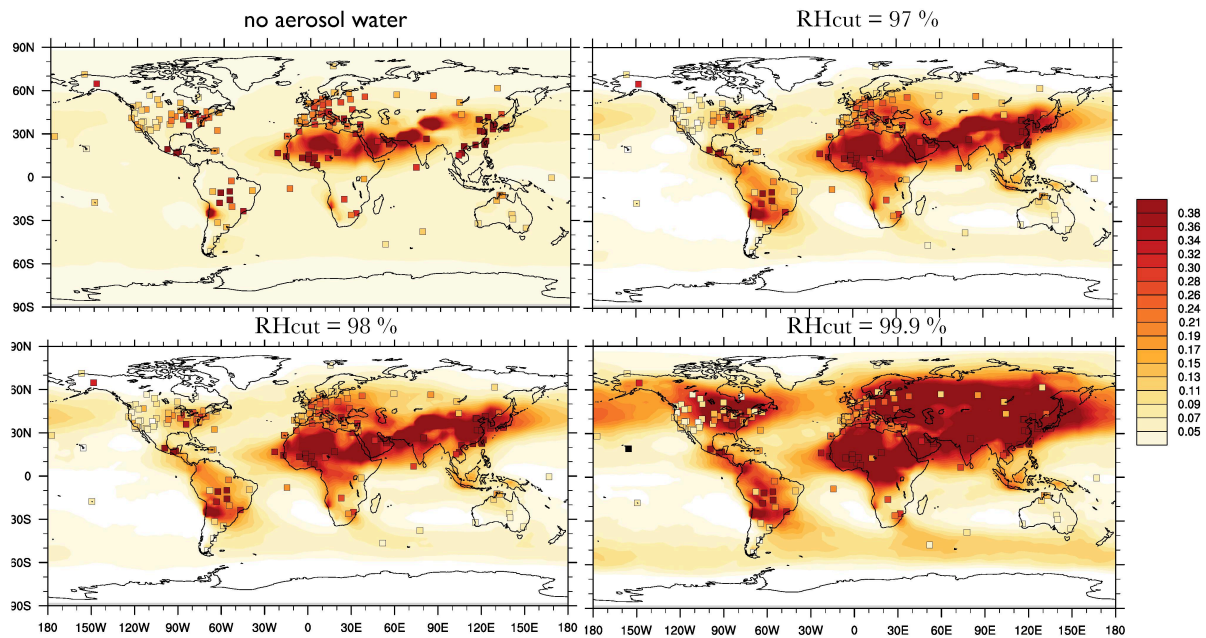
Figure 15. Sensitivity of EMAC AOD to different RH cut-offs (see text Sec. 4.3).